Novel role for the midbody in primary ciliogenesis by polarized epithelial cells

Miguel Bernabé-Rubio,[1] Germán Andrés,[2] Javier Casares-Arias,[1] Jaime Fernández-Barrera,[1] Laura Rangel,[1] Natalia Reglero-Real,[1] David C. Gershlick,[3] José J. Fernández,[4] Jaime Millán,[1] Isabel Correas,[1] David G. Miguez,[5] and Miguel A. Alonso[1]

[1]Department of Cell Biology and Immunology and [2]Electron Microscopy Unit, Centro de Biología Molecular Severo Ochoa, Consejo Superior de Investigaciones Científicas and Universidad Autónoma de Madrid, 28049 Madrid, Spain
[3]Cell Biology and Neurobiology Branch, Eunice Kennedy Shriver National Institute of Child Health and Human Development, National Institutes of Health, Bethesda, MD 20892
[4]Centro Nacional de Biotecnología, Consejo Superior de Investigaciones Científicas, 28049 Madrid, Spain
[5]Department of Condensed Matter Physics, Instituto de Ciencias de Materiales Nicolás Cabrera and Instituto de Física de la Materia Condensada, Universidad Autónoma de Madrid, 28049 Madrid, Spain

The primary cilium is a membrane protrusion that is crucial for vertebrate tissue homeostasis and development. Here, we investigated the uncharacterized process of primary ciliogenesis in polarized epithelial cells. We show that after cytokinesis, the midbody is inherited by one of the daughter cells as a remnant that initially locates peripherally at the apical surface of one of the daughter cells. The remnant then moves along the apical surface and, once proximal to the centrosome at the center of the apical surface, enables cilium formation. The physical removal of the remnant greatly impairs ciliogenesis. We developed a probabilistic cell population–based model that reproduces the experimental data. In addition, our model explains, solely in terms of cell area constraints, the various observed transitions of the midbody, the beginning of ciliogenesis, and the accumulation of ciliated cells. Our findings reveal a biological mechanism that links the three microtubule-based organelles—the midbody, the centrosome, and the cilium—in the same cellular process.

Introduction

Most vertebrate cells have a primary cilium (PC) that projects from their surface as a single appendage (Gerdes et al., 2009; Bornens, 2012). The PC orchestrates important signaling pathways involved in development and cell proliferation, differentiation, survival, and migration (Singla and Reiter, 2006; Goetz and Anderson, 2010). Ciliary dysfunction produces a great variety of human developmental and degenerative disorders, collectively known as ciliopathies, which can affect nearly every major organ in the body (Hildebrandt et al., 2011).

In mammals, the PC consists of a specialized membrane protrusion that surrounds a structure known as the axoneme, which is organized in a ninefold symmetrical arrangement of microtubule doublets. In some cell types, the PC is deeply rooted in the cytoplasm in a membrane invagination referred to as the ciliary pocket, whereas in others the PC directly protrudes from the plasma membrane (Rohatgi and Snell, 2010; Benmerah, 2013). It has been postulated that the presence or absence of the ciliary pocket is a consequence of the use of two distinct pathways of primary ciliogenesis (Benmerah, 2013), distinguished by the position of the centrosome, either near the nucleus or close to the cell apex (Sorokin, 1968). In fibroblasts, which have a ciliary pocket and the centrosome near the nucleus, ciliogenesis follows the intracellular route, which begins inside the cell with the progressive formation of a large ciliary vesicle that encapsulates the distal end of the mother centriole. This vesicle is usually thought to be of Golgi origin, although, at least in embryonic neocortical stem cells, it appears that can also be derived from a previous ciliary membrane (Paridaen et al., 2013). After formation of an incipient axoneme by elongation of the two inner microtubules from each of the nine microtubule triplets of the mother centriole, the ciliary vesicle fuses with the plasma membrane and gives rise to the ciliary membrane and, probably, the ciliary pocket (Sorokin, 1962). In contrast, cells such as renal polarized epithelial cells (Latta et al., 1961), which lack a ciliary pocket and have their centrosome at the cell apex, assemble a PC once the centrosome is positioned at the cell apex. Despite its fundamental relevance, research on primary ciliogenesis has concerned itself almost

Correspondence to Miguel A. Alonso: maalonso@cbm.csic.es

Abbreviations used: IFT, intraflagellar transport; IMCD3, inner medullary collecting duct 3; MKLP1, mitotic kinesin-like protein 1; PC, primary cilium; PRC1, protein required for cytokinesis 1; RPE1, retinal pigment epithelial 1; TUSP, take-up by suction pressure.

The Rockefeller University Press $30.00
J. Cell Biol. Vol. 214 No. 3 259–273
www.jcb.org/cgi/doi/10.1083/jcb.201601020

exclusively with the intracellular pathway, whereas the existence of an alternative route in polarized epithelial cells has remained largely unexplored.

Cytokinesis begins with ingression of the cleavage furrow that progressively constricts the cytoplasm and transforms spindle microtubules into the intercellular bridge connecting the two daughter cells (Chen et al., 2012; Fededa and Gerlich, 2012; Green et al., 2012). The midbody, or Flemming body, which is a 1.0- to 1.5-µm-electrodense structure characterized by dense packing of overlapping antiparallel microtubule bundles, forms in the middle of this bridge. Severing of the bridge membrane on one side of the midbody results in the physical separation of the two daughter cells. Once this process has taken place, if the bridge is severed on the other side, the postmitotic midbody is shed into the extracellular milieu and deteriorates with time. Alternatively, in the event that the second scission does not occur, the midbody is asymmetrically inherited by one of the daughter cells as a remnant, to be degraded or conserved over an extended period (Marzesco et al., 2005; Pohl and Jentsch, 2009; Kuo et al., 2011; Salzmann et al., 2014). The position of the remnant marks the site of formation of the first neurite in *Drosophila melanogaster* neurons in vivo (Pollarolo et al., 2011), defines the place of initiation of lumen formation in epithelial cells (Li et al., 2014), and constitutes a landmark for defining dorsoventral axis formation during the early development of *Caenorhabditis elegans* (Singh and Pohl, 2014). Although the exact role of the midbody remnant in these processes remains a mystery, its importance in cellular physiology and determination of cell fate is becoming apparent (Chen et al., 2013; Dionne et al., 2015).

Epithelial Madin-Darby canine kidney (MDCK) cells constitute a paradigm of renal tubular epithelial cells extensively used for investigating specialized membrane trafficking mechanisms and in vitro tubule formation (Rodriguez-Boulan et al., 2005). Here, we used MDCK cells to investigate the process of primary cilium formation in polarized renal epithelial cells. We show that the midbody remnant of MDCK cells is retained by one of the daughter cells and becomes located at the apical surface close to the cell junctions. The midbody remnant, which carries important machinery for primary cilium formation, such as Rab8 and intraflagellar transport (IFT) and exocyst subunits, then moves along the apical surface to the central zone, where the centrosome is situated. Once there, a primary cilium emerges. If the remnant is removed, primary ciliogenesis is greatly impaired. A mathematical simulation explains the dynamics of the process in terms of constraints on cell area brought about by cell proliferation and establishment of cell–cell contacts. Our work reveals a new biological mechanism for the process of primary ciliogenesis that directly implicates the postmitotic midbody.

Results

The effect of confluence and quiescence on primary ciliogenesis appears to depend on the cell type and cell culture conditions (Wheatley et al., 1994; Alieva and Vorobjev, 2004). MDCK cells form a PC at the center of the apical membrane when they are grown at high cell density, but unlike other cells, they do not form a PC in response to serum deprivation. The PC of MDCK cells does not contain a ciliary pocket (Zuo et al., 2009; Reales et al., 2015), and the centrosome of nonciliated cells localizes close to the apical membrane and is devoid of a large ciliary vesicle (Fig. 1, A and B). Therefore, as such, MDCK cells are an appropriate model for investigating the existence of an alternative pathway of ciliogenesis. The machinery for IFT (Rosenbaum and Witman, 2002), the Rab GTPase Rab8, and exocyst (a multi-subunit complex involved in tethering vesicles to the plasma membrane [Heider and Munson, 2012]) are important for the assembly of the PC (Nachury et al., 2007; Zuo et al., 2009; Das and Guo, 2011). To understand ciliogenesis in MDCK cells, we first examined the distribution at the apical zone of IFT20, a component of the IFT machinery. Interestingly, in addition to its expected ciliary localization, in nonciliated cells, IFT20 concentrated in a tubulin-rich structure positioned at the apical surface either peripherally, close to the cell junctions, or centrally, close to the centrosome (Fig. 1 C). Rab8 (Fig. 1 D) and Exo70 (Fig. S1 A; a subunit of the exocyst complex), but not podocalyxin (a PC-excluded transmembrane protein [Meder et al., 2005]; Fig. 1 E), also distributed in the three apical patterns. IFT88 followed the same distribution patterns (Fig. S1 B), but IFT81 (Fig. S1 C) was detected only in ciliary structures. Quantifying the number of cells with each of the three profiles in growing cells evolving from low to high confluence showed that cells with a peripheral profile emerged first, followed by the cell population with a central profile and then those with a cilium (Fig. 1 F). These dynamics and the observation that the PC shares IFT20, Rab8, Exo70, and α-tubulin with the central and peripheral structures prompted us to characterize these structures, examine their relationship, and investigate their involvement in ciliogenesis.

During cytokinesis, the intercellular bridge connecting newly formed daughter cells forms at the apical surface of MDCK cells (Reinsch and Karsenti, 1994; Fig. 2, A and B; and Video 1). The physical separation of the daughter cells then takes place by a process called abscission, which involves disassembly of the microtubules adjacent to the midbody and scission of the membrane bridge (Chen et al., 2012; Fededa and Gerlich, 2012; Mierzwa and Gerlich, 2014). After abscission, the postmitotic midbody was inherited as a midbody remnant by one of the daughter cells and localized at the apical surface close to the junction between them (Fig. 2 A and Video 1). The peripheral structure positive for IFT20 was identified as a midbody remnant by its colocalization with protein required for cytokinesis 1 (PRC1; Jiang et al., 1998; Fig. 2 C) and mitotic kinesin-like protein 1 (MKLP1; Mishima et al., 2002; Fig. S1 D), which were used as endogenous markers of the midbody, and with exogenous GFP-PRC1 (Fig. S1 E). The characteristic microtubular pattern and electrodense ultrastructure seen by EM analysis of the peripheral profiles confirmed this assignment (Figs. 2 D and Fig. S2, A and B). It is of note that detailed analysis of serial sections indicates that peripheral remnants are connected to the rest of the cell through tethers that appear continuous with the midbody (Fig. 2 D).

Consistent with previous observations in HeLa cells (Kaplan and Reiner, 2011), Rab8 was found in the intercellular bridge in MDCK cells, as was IFT88 (Fig. S1 F). IFT20 and IFT88 were also detected in the bridge in human telomerase reverse transcription–immortalized retinal pigment epithelial 1 (RPE1) cells (Fig. S1 G), which have a ciliary pocket and follow the intracellular route of ciliogenesis (Molla-Herman et al., 2010). Because IFT20 had not previously been detected in the bridge (Follit et al., 2006), its presence was confirmed by expression of GFP-IFT20 (Fig. S1 H). The localization of Rab8, IFT20, and IFT88 in the intercellular bridge explains their presence in peripheral remnants.

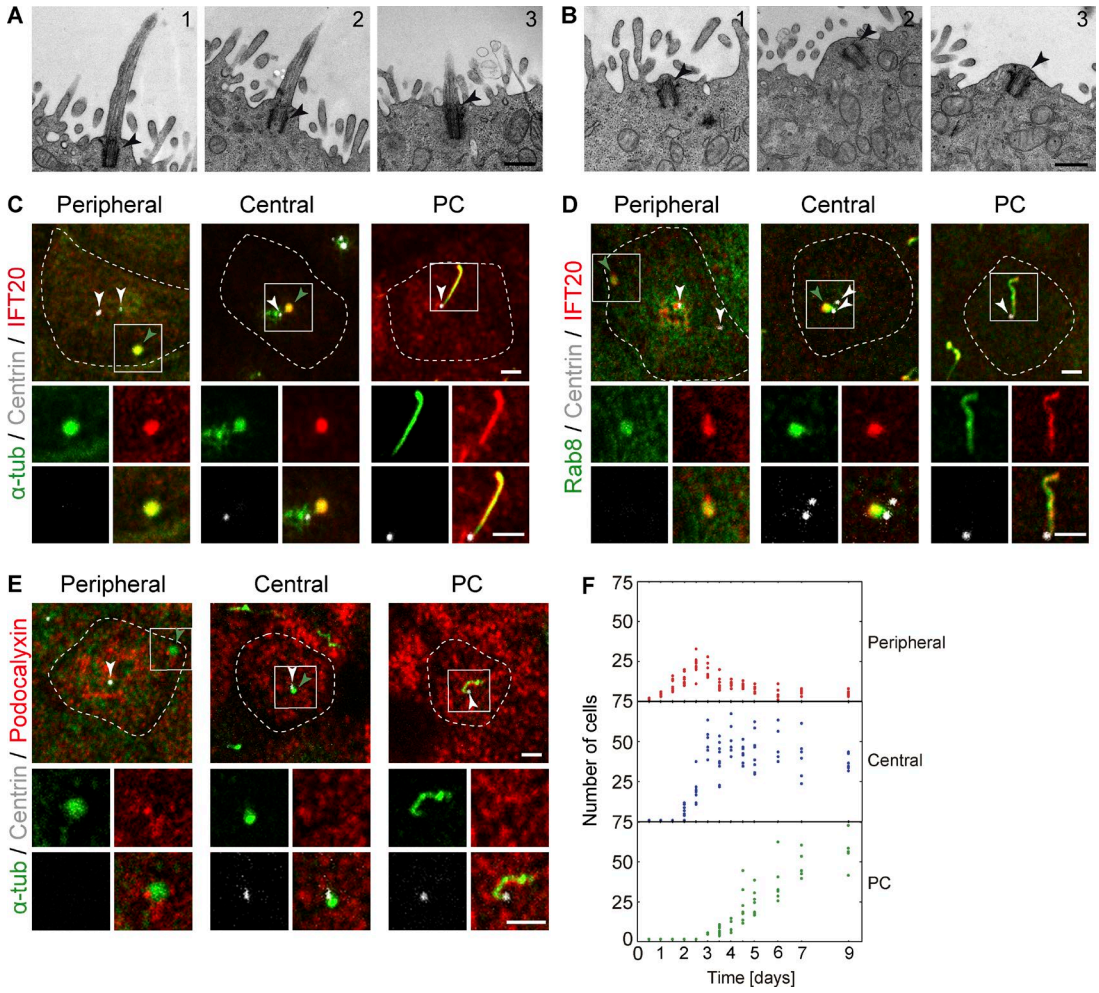

Figure 1. **IFT20 and Rab8 concentrate at peripheral and central structures in nonciliated MDCK cells.** (A and B) EM micrographs showing three representative examples of PCs (A) and apical centrosomes (B). No ciliary pocket (A) or vesicles surrounding the centrosome (B) were observed in 14 cilia and 16 apical centrosomes examined, respectively. The arrowhead marks the centrosome. Bars, 500 nm. (C–E) Cells grown for 4 d were stained for IFT20 and α-tubulin (C), Rab8 and IFT20 (D), and podocalyxin and α-tubulin (α-tub; E). The position of the centrosome was monitored by expression of dsRed-centrin. The projection of one to three apical planes of one representative example of each of the distributions patterns is shown. The dashed line indicates the cell contour. The enlargement shows the fluorescent signal in the boxed region for the proteins analyzed. White arrowheads point to the centrosome or to each of the two centrioles if they are separated, and green arrowheads point to the peripheral and central structures. Bars, 2 µm. (F) The number of cells with peripheral or central structures or a PC was measured at the indicated times after cell plating. Each dot represents the result from a microscope field. Three independent experiments were performed (n = 207–847 cells per time point; two to five fields per time point and per experiment).

To determine whether the central profile arises from translocation of the peripheral remnant, we tracked the dynamics of peripheral remnants labeled with GFP-PRC1 and cherry-tubulin. We observed that the remnant moved along the apical surface toward the center of the apical membrane (Fig. 3 A and Video 2). We also used cells expressing GFP-tubulin and dsRed-centrin to confirm that the remnant moves to be proximal to the centrosome (Fig. 3 B and Video 3). The transition to become cells with a central remnant occurred in ∼72% of cells that had a peripheral remnant, as measured 60–72 h after cell seeding, and the journey took 1–4 h, as assessed by videomicroscopic analysis of 40 cells. It is of note that the remnant reached a central position by climbing along the apical surface as the cell gradually grew in height and occupied less area (Fig. 3 C and Video 4). Similar to what was observed in peripheral remnants (Figs. 2 D and S2 A), EM analysis of serial longitudinal cell sections of a remnant in the proximity of the centrosome showed that the remnant is connected to the rest of the cell by a thin stalk (Fig. 3, D [section S2′] and E; and Fig. S3 B). In addition, the 3D reconstruction of serial EM sections showed that the midbody remnant is closely embraced by microvilli (Fig. 3 E and Video 5).

Rab8 localizes to the PC and is essential for efficient PC formation in RPE1 cells (Nachury et al., 2007; Westlake et al., 2011; Kuhns et al., 2013). The midbody remnant transports Rab8 to the center of the apical membrane in MDCK cells (Fig. S3 A). To investigate whether Rab8 is necessary for the movement of the remnant, we silenced Rab8 expression with specific siRNA (Fig. S4, A and B). Rab8 knockdown produced the accumulation of peripheral remnants in MDCK cells and, as in cells with a ciliary pocket, compromised PC formation (Fig. 4, A and B). This effect was impeded in cells expressing exogenously human Rab8 (Fig. 4, C and D). As a control of the specificity of the effect of Rab8 knockdown on the movement of the remnant, we observed that IFT88 knockdown (Fig. S4, C and D) did not produce the same effect (Fig. 4, E and F). Instead, IFT88 knockdown reduced the number not only of ciliated cells, but also of peripheral remnants, probably by favoring remnant release.

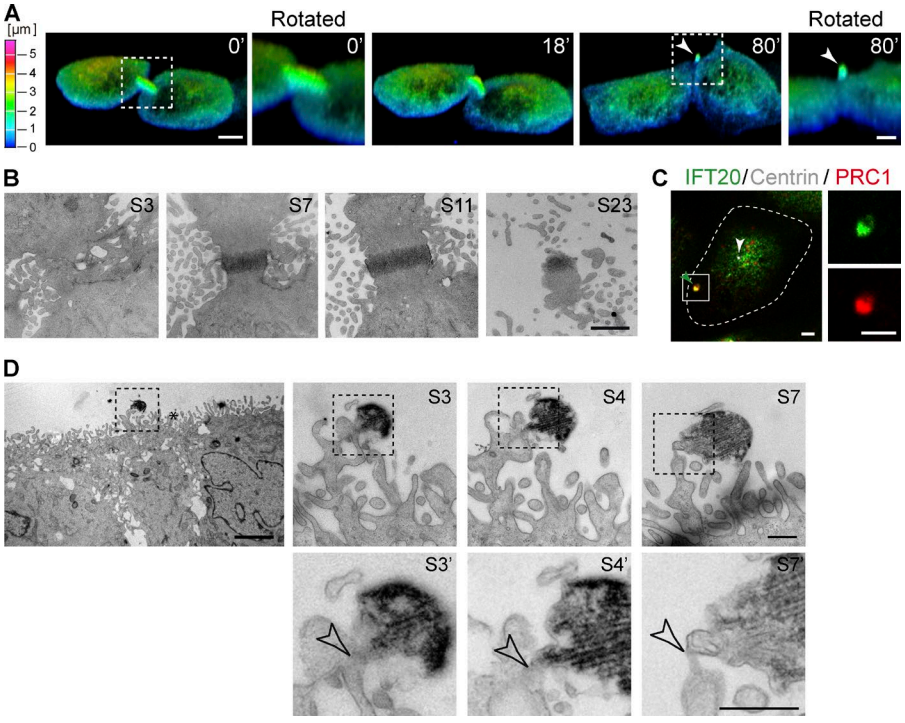

Figure 2. **The peripheral structure containing ciliary markers is a postmitotic midbody.** (A) The images correspond to 3D reconstructions of cells expressing cherry-tubulin that were filmed during cell division. The images were pseudocolored based on height, using the color scale on the left, to highlight that the intercellular bridge forms at the top of the cells and that the postmitotic midbody remnant localizes after abscission at a peripheral position at the apical surface. The arrowhead points to the postmitotic midbody. Bar, 5 µm. An enlargement of the boxed region at 0 and 80 min is also shown. Bars, 2 µm. (B) Serial EM sections of the apical region of MDCK cells during cytokinesis. The sections are numbered S1 onwards from the lower section to the top. Note the progressive loss of microvilli at the top sections. Bar, 1 µm. (C) Cells expressing dsRed-centrin were stained for IFT20 and PRC1. The enlargement of the boxed region shows the fluorescent signal for IFT20 and PRC1. The dashed line indicates the cell contour. The white and green arrowheads point to the centrosome and the peripheral structure, respectively. Bars, 2 µm. (D) EM micrograph of a cell with a peripheral midbody remnant (left panel) and enlargements of different serial sections (S3, S4, and S7, right). Note that in some of the sections it appears that the remnant is connected to the rest of the cell by a thin tether (empty arrowhead) as shown in the enlargements of the boxed regions of sections S3, S4, and S7 (S3′, S4′, and S7′, bottom). Asterisks indicate cell junctions. The images are orthogonal serial sections from the same cell. The sections were numbered S1 onwards from the back to the front. Bars: (panoramic view) 3 µm; (enlargements) 500 nm.

In addition, Rab8 knockdown did not grossly alter the process or duration of cytokinesis (Fig. S4, E and F). Although Rab8 regulates the establishment of apico-basal polarity and membrane trafficking, expression of dominant negative Rab8 does not produce loss of cell polarity in monolayers of already polarized cells (Ang et al., 2003). Similarly, we found that cell polarity, as assayed by the steady-state distribution of the apical podocalyxin and basolateral β-catenin markers and that of the tight junction ZO-1 protein, was apparently normal in the absence of Rab8 (Fig. S4 G). As in the case of peripheral remnants of normal cells, analysis of serial EM sections showed that the remnants of Rab8-knockdown cells were connected to the apical membrane by a thin stalk that appears continuous with the midbody (Fig. 4 G and Fig. S4 H). In summary, the results in Fig. 4 show that the midbody remnant moves along the apical membrane from a peripheral position toward the centrosome in a Rab8-dependent manner.

Having established that the central structure corresponded to the midbody remnant, we investigated the relationship between the central remnant and the cilium. Videomicroscopic analysis and 3D reconstruction of cells coexpressing GFP-tubulin and dsRed-centrin (Fig. 5 A and B; and Video 6) further revealed that a PC starts assembling once the remnant has encountered the centrosome. The observation of this encounter between the remnant and the centrosome could be reproducibly observed (n = 10 cells). A thin microtubular connection between the two structures preceded formation of a nascent cilium (Fig. 5 A). A second example of this microtubular extension is presented in Fig. 5 C. Afterward, the midbody remnant progressively separated from the centrosome and was eventually lost (Fig. 5 A). Similarly, movement of the midbody remnant to the cell center and PC formation were observed in inner medullary collecting duct 3 (IMCD3) cells (Fig. S4, I and J), where it is known that ∼90% of ciliated cells lack a ciliary pocket (Molla-Herman et al., 2010). In summary, the results in Figs. 3 and 5 are compatible with a sequential process by which the daughter cell that inherits the midbody remnant forms a PC by a process involving the movement of the remnant along the apical surface to become proximal to the centrosome.

Because of its dense structure and large size, the energy needed to destroy a midbody by laser ablation is so high that it causes extensive cell damage. Therefore, to investigate directly the requirement of the midbody remnant for PC biogenesis, we designed a gentle procedure to physically remove it. The procedure, which was named "take-up by suction pressure" (TUSP), uses patch-clamp equipment to aspirate the remnant (Fig. 6 A and Video 7). As a control, the same procedure was performed in cells with a remnant in a zone of the plasma membrane distant from it. Removal of the remnant by TUSP resulted in a fourfold reduction in the number of PCs relative to control cells (Fig. 6, B and C). Approximately 20% of the cells still formed a PC despite having their remnant removed, indicating that remnant removal might not have been complete in those cells, that the remnant had already enabled the centrosome to form a PC before removal, or that they formed a PC in a midbody remnant–independent manner. As controls of the TUSP procedure, we observed that cell polarity, as determined by the distribution of podocalyxin, β-catenin, and ZO-1 (Fig. 6 D) and F-actin and

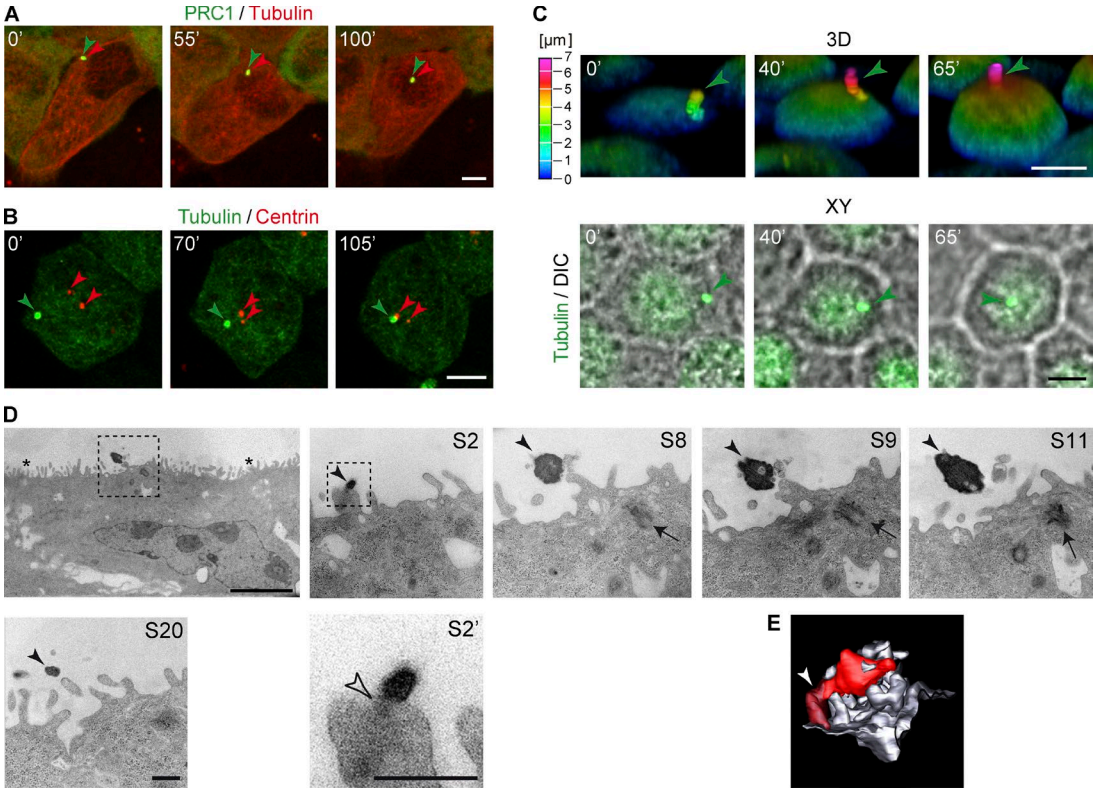

Figure 3. **The midbody remnant moves along the apical surface from a peripheral to a central position to encounter the centrosome.** (A and B) XY confocal stack of cells coexpressing GFP-PRC1 and cherry-tubulin (A) and GFP-tubulin and dsRed-centrin (B) during movement of the midbody remnant. In A, the green and red arrowheads point to the midbody remnant pools of PRC1 and tubulin, respectively. In B, the green and red arrowheads point to the remnant and the centrioles, respectively. (C) 3D reconstruction of cells expressing GFP-tubulin during remnant movement (top). The images were pseudocolored based on height, using the color scale on the left, to highlight that the remnant moved to the center of the apical surface as the cell gained height. The green arrowhead points to the midbody remnant. The differential interference contrast (DIC) images show that the cell occupied 25% less area at the end (bottom). Bars, 5 µm. (D) EM micrograph of a cell with the remnant in the vicinity of the centrosome at the center of the apical surface and enlargements of different sections. The images are orthogonal serial sections from the same cell. Asterisks indicate cell junctions, the black arrowhead points to the remnant, and the arrow indicates the centrosome. The sections were numbered S1 onwards from the back to the front. Note that it appears that the remnant is connected to the rest of the cell by a thin tether, indicated by an empty arrowhead (see S2′, which is an enlargement of the boxed region of S2). Bars: (panoramic view) 4 µm; (enlargements) 500 nm. (E) 3D reconstruction of the central remnant (red), the tether (dark red), and adjacent apical membrane (gray) obtained by manual tracing and stacking of their contours after alignment of the serial EM sections of Fig. S3 B. The arrowhead indicates the tether.

β-catenin (Fig. S5 A), and integrity of the plasma membrane, as assessed with a biotinylation reagent that does not permeate the plasma membrane (Fig. S5 B), were normal in cells in which TUSP was used for remnant removal. Cells remained viable as they responded to hepatocyte growth factor by undergoing cycles of extension-retraction of their plasma membrane, as did control cells in the same microscope field (Video 8). In summary, the results in Fig. 6 show that the midbody remnant is essential for efficient primary ciliogenesis.

Quantification of the area of the substrate occupied by the cells (hereafter referred to as the cell area) indicated that whereas the area of the cells with a peripheral remnant was not restricted, the cells with a central remnant or a primary cilium had areas less than 400 and 200 µm^2, respectively (Fig. 7 A). To investigate the possibility that constraints in the cell area regulate the process of PC formation, we developed a probabilistic population-based mathematical model in which cells are allowed to proliferate and transit between the different stages solely on the basis of the value of the cell area. In addition to the results in Fig. 7 A, the model was designed on the basis of parameters derived from measurements of the total cell number (Fig. 7 B), the single-cell area over time (Fig. S5, C–E), and the number of cells with a midbody remnant or a ciliary structure (Fig. 7 C). We defined the various transitions observed (cell cycle length, remnant conservation, movement of the remnant from a peripheral to a central position, and start of ciliogenesis) in the form of Hill functions of the cell area (Fig. 7 D and Materials and methods). The resulting simulations (Fig. 8 A) show that cells with a peripheral remnant emerged first, followed by the cell population with a central remnant and then those exhibiting a ciliary structure. This is consistent with our videomicroscopic analyses indicating a sequential relationship between the profiles. The simulations closely reproduced the experimental data of Fig. 1 F, as shown by their superimposition (Fig. 8 B). This finding indicates that constraints in the cell area explain all the experimentally observed transitions.

We used the micropatterning method to confirm that the cell area controls the different transitions of the midbody remnant and PC formation. A single cell was plated on disk micropatterns of 700, 1,100, and 1,600 µm^2 (Fig. 8 C), and the cell was left to divide to generate four or eight to 12 cells covering the entire available surface of the disks (Fig. 8 D). Consistent with the simulations, the percentage of cells with a midbody remnant or a PC increased as the cell area became smaller (Fig. 8 E). Moreover, the percentage of cells with either a central remnant or a PC increased with the degree of cell confinement (Fig. 8 F).

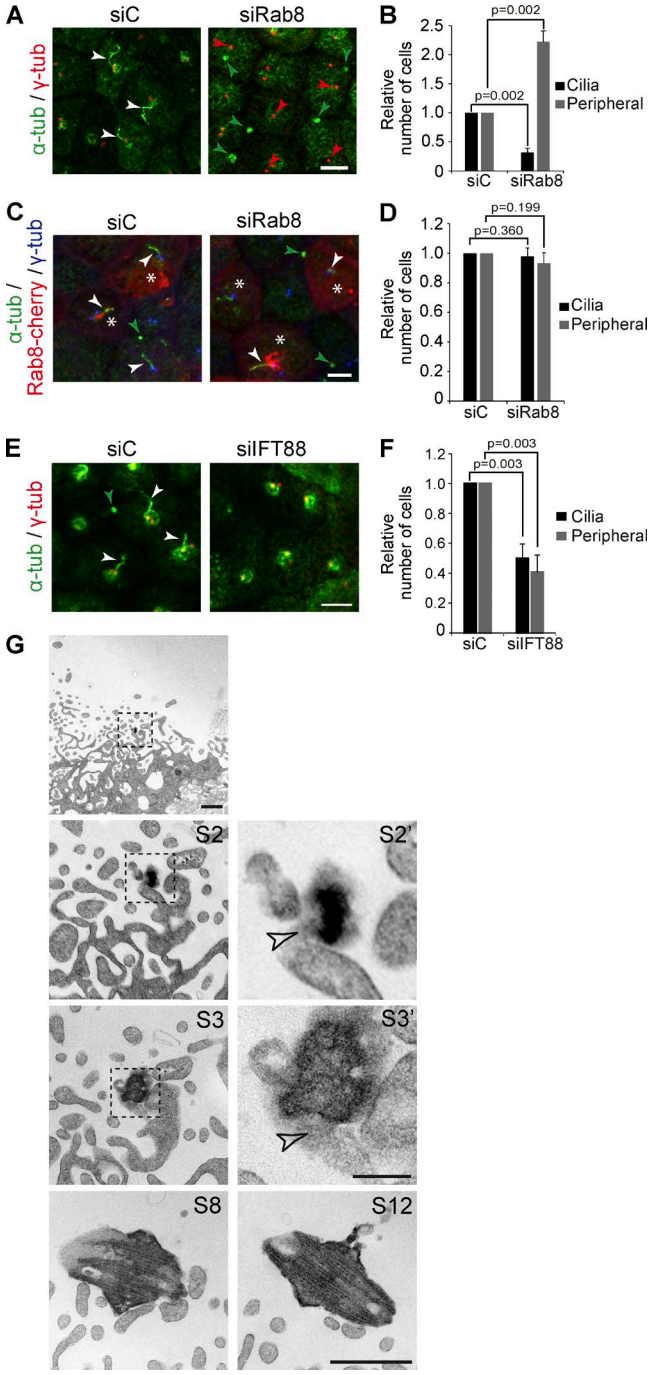

Figure 4. **Rab8 is necessary for the movement of the midbody remnant.** (A–D) Control cells (A and B) or cells stably expressing cherry-Rab8 (C and D) were transfected with siRNA control (siC) or targeted to Rab8 (siRab8). (A and C) Cells were stained for α- and γ-tubulin (α- and γ-tub). The green and red arrowheads point to the midbody remnant and the centrosome, respectively. The white arrowheads indicate the PCs. The asterisks in C mark the cells expressing cherry-Rab8. (B) The number of cells with a peripheral remnant or a PC was quantified in Rab8-knockdown cells and was expressed relative to that in siC-transfected cells. Data represent the mean + SEM from three independent experiments (n = 381 control cells and 354 Rab8-knockdown cells; two to three fields per experiment; Student's t test). (D) The number of cells with a peripheral remnant or a PC was quantified in siRab8-transfected cells expressing cherry-Rab8 and was expressed relative to that in siC-transfected cells. Data represent the mean + SEM from three independent experiments (n = 294 control cells and 322 Rab8-knockdown cells; three fields per experiment; Student's t test). (E and F) Cells were transfected with siC or siIFT88. (E) Cells were stained for α- and γ-tubulin. The green and white arrowheads point to the midbody remnant and the PC, respectively. (F) The number of cells with a peripheral remnant or a PC in IFT88-knockdown cells is expressed relative to that in siC-transfected cells. Data represent the mean + SEM from three independent experiments (n = 1,201 control cells and n = 1,329 IFT88-knockdown cells; three fields per experiment; Student's t test). (G) Panoramic EM image of an apical zone with a midbody remnant in a Rab8-knockdown cell (top) and enlargements of serial sections of the remnant region from the same cell. The sections were numbered S1 onwards from the bottom to the top. Panels S2′ and S3′ show an enlargement of the boxed regions in S2 and S3, respectively. Note that it appears that the remnant is connected to the rest of the cell by a thin tether, indicated by an empty arrowhead. Bars: (A, C, and E) 5 µm; (G, panoramic view and S2–S12) 1 µm; (G, S2′ and S3′) 200 nm.

It is of note that this increase did not affect all the cells on the disk in the same manner: cells at the edge had preferentially peripheral remnants, whereas those in an internal position exhibited most of the central remnants and PCs (Fig. 8 G). This observation is consistent with our measurements on cells grown on coverslips (Fig. 1 F), since in that analysis we ignored the cells at the edge of the coverslip. One interpretation of these findings is that, in addition to a reduced cell area, cell–cell contact favors the transitions of the midbody remnant and PC formation to occur efficiently.

Based on mathematical simulations, and supported by our experimental data, we propose a model of primary ciliogenesis that is mediated by the midbody remnant in which the transitions of the remnant (loss or movement to a central position) and the beginning of the ciliogenesis process are controlled in a cell area–dependent manner by two cell area thresholds (Fig. 9). It is of note that the first threshold (~400 µm^2), which marks the transition from a peripheral to a central remnant, approximately coincides with the area of cells reaching confluence (Fig. S5 F). The second threshold (~200 µm^2) marks the transitions to quiescence, full conservation of the remnant after cell division, and the beginning of ciliogenesis. Under our experimental conditions, most cells at day 9 (72.6 ± 10.2%) had a midbody remnant and hence had the potential to eventually form a PC, or had already formed a PC. Achieving higher percentages of ciliated cells requires an increase in the percentage of cells with one midbody remnant by new cycles of cell division or the elimination of the pool of cells without a remnant. Alternatively, the remaining cells simply might not be able to ciliate, as occurs with a pool of 10% of IMCD3 cells, or to assemble a PC by the intracellular route, which is probably the case of the pool of 10% of ciliated IMCD3 cells that have a ciliary pocket (Molla-Herman et al., 2010).

Discussion

Our understanding of the process of primary ciliogenesis in polarized epithelial cells has advanced little since the classic EM work of Sorokin nearly 50 years ago. In that seminal contribution, it was proposed that in polarized epithelial cells, primary ciliogenesis occurs on the plasma membrane, unlike in other cell types, such as fibroblasts and smooth muscle cells, in which cilium assembly starts intracellularly (Sorokin, 1968). In this article, we have analyzed the process of primary ciliogenesis in polarized MDCK epithelial cells. We show that, once the sister cells have separated, the postmitotic midbody locates peripherally at the apical surface for up to 4–10 h and concentrates machinery important for primary cilium growth, such as the Rab8,

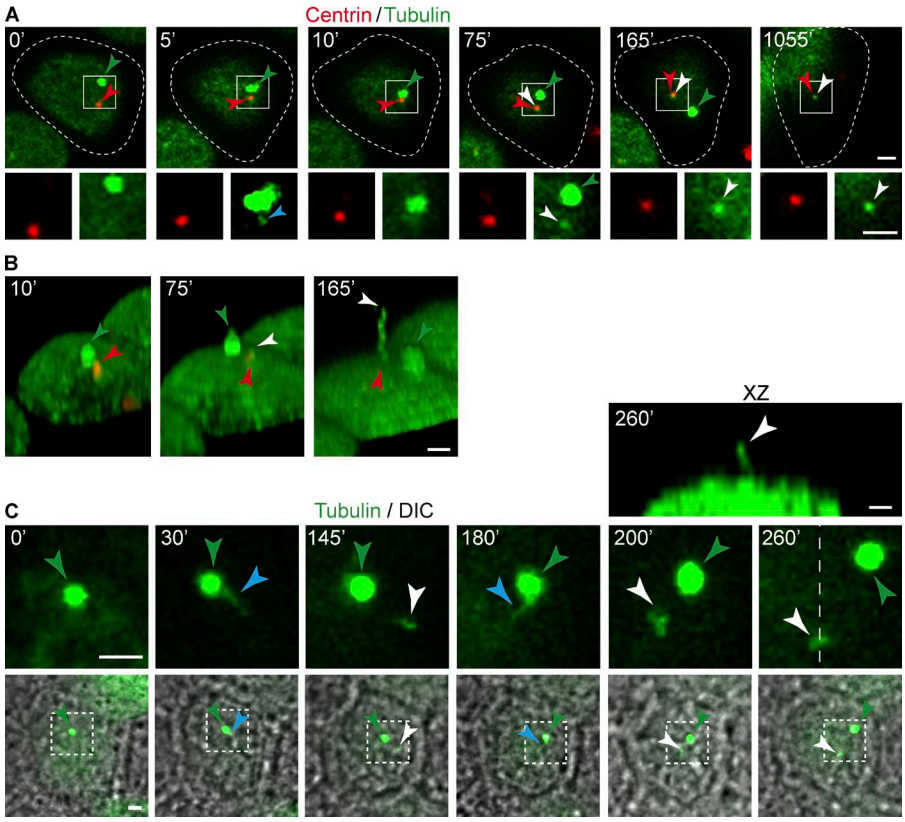

Figure 5. **A primary cilium forms once the midbody remnant becomes proximal to the centrosome.** (A–C) Videomicroscopic analysis of PC formation. (A) XY projection of GFP-tubulin and dsRed-centrin during PC formation (top). The enlargements show the fluorescent signal in the boxed region for the proteins analyzed (bottom). The blue and white arrowheads indicate a microtubular connection between the midbody remnant and the centrosome and a nascent cilium, respectively. The green and red arrowheads point to the midbody remnant and the centrosome, respectively. The dashed line indicates the cell contour. (B) 3D reconstruction of some of the images shown in A. (C) XY projection of GFP-tubulin and their corresponding differential interference contrast (DIC) images during PC formation (bottom). The enlargement of the boxed region shows the distribution of tubulin at apical planes (middle). Nascent cilia are visualized in the XY projections as dots because they are perpendicular to the substrate. Green arrowheads point to the midbody remnant. The blue and white arrowheads indicate a microtubular extension similar to that observed in A and a nascent cilium, respectively. An XZ image of the cells after 260 min is included to show that the new profile that appears close to the midbody remnant (white arrowhead) is a nascent cilium (top). The dotted line indicates the plane used for the confocal XZ image. Bars, 2 µm.

IFT, and exocyst components. The postmitotic midbody remnant then moves along the plasma membrane over 1–4 h carrying this machinery toward the center of the apical surface where the centrosome is situated. Primary cilium formation begins once the two organelles have been proximal for 2–6 h. Therefore, under our experimental conditions, the remnant remains associated with the cell membrane for 7–20 h before primary cilium assembly. Removal of the remnant greatly interferes

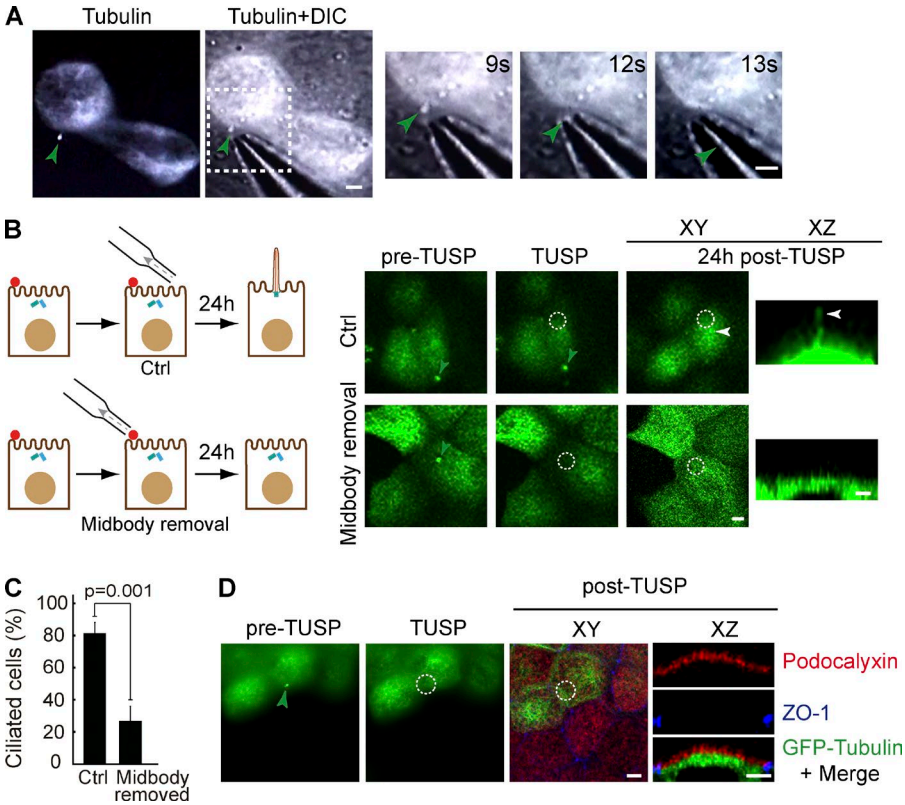

Figure 6. **Removal of the midbody remnant greatly interferes with PC formation in MDCK cells.** (A) Representative images of the TUSP procedure. DIC, differential interference contrast; (B and C) TUSP was used to remove the midbody remnant (B, bottom). As a control (Ctrl), TUSP was applied to cells with a remnant in a zone of the plasma membrane distant from it (B, top). After 24 h, the same cells were examined for the presence of a PC. The green and white arrowheads mark the midbody remnant and the PC, respectively. The circles indicate the plasma membrane zone subjected to TUSP. Bars, 3 µm. (C) The percentage of ciliated cells was quantified 24 h post-TUSP. Data represent the mean + SEM from six independent experiments (n = 26 control cells and 27 cells whose midbody remnant was removed; χ^2 test). (D) The distribution of podocalyxin, ZO-1, and GFP-tubulin was analyzed in cells in which the remnant was removed by TUSP. The arrowheads point to the midbody remnants, and the circles mark the plasma membrane zone subjected to TUSP. Bars, 5 µm.

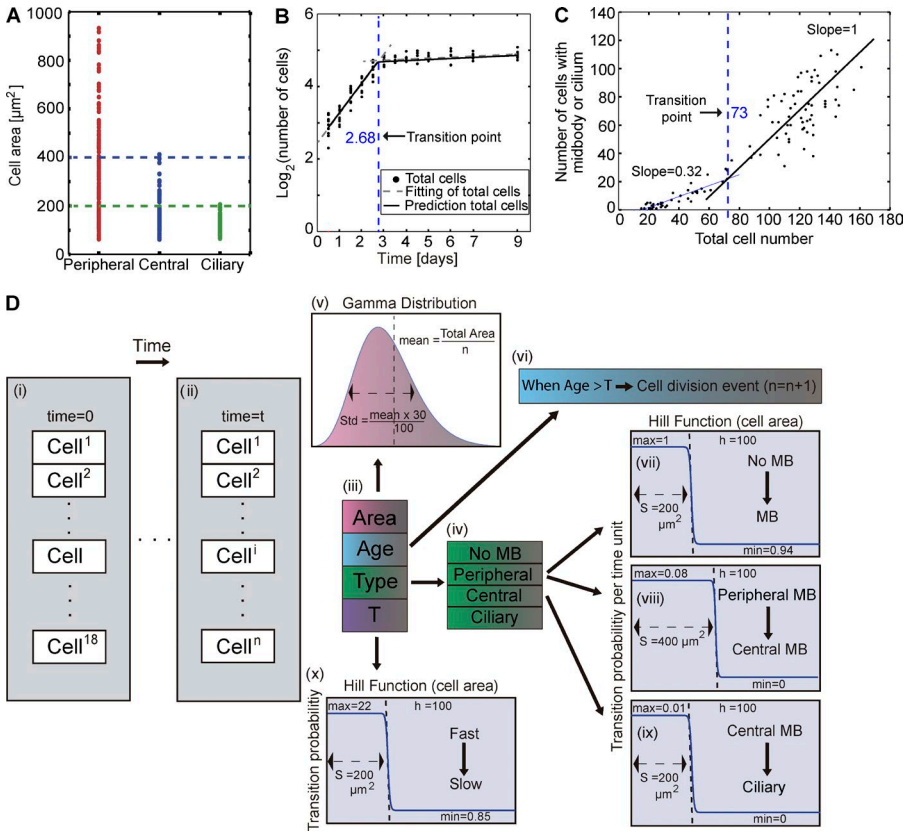

Figure 7. **Development of a mathematical model of primary ciliogenesis.** (A) Plot of the single-cell measures of cell area for peripheral, central, and ciliary profiles. Three independent experiments were performed (n = 406 cells; two to five fields per experiment were examined). (B) Plot of the total number of cells (black dots) over time. Fitting of "fast" and "slow" dynamics (gray dashed lines) intersects at the transition point (2.68 d). Prediction of the total number of cells by a Hill function of the cell cycle using a Hill coefficient of 100 (solid black line). (C) Plot of the number of cells with midbody remnant or PC versus the total number of cells. Two dynamic regimens that intersect at a total number of ∼73 cells are distinguished. Slope values less than 1 mean that a fraction of the new cells in the system does not conserve the remnant. Three independent experiments were performed (n = 207 to 847 cells per time point; two to five fields per time point and per experiment) in B and C. (D) Rationale of the probabilistic population-based mathematical model. (i and ii) An initial set of cells is allowed to proliferate and develop up to a given time t. (iii) Each individual cell in the population is defined as a numerical entity with four variables: its area, age, type, and cell cycle length (T). (iv) Cells can be in one of four distinct configurations depending on whether they lack or have a midbody remnant (MB) in a peripheral or central position or a ciliary structure. These configurations were named as no MB, peripheral, central, and ciliary, respectively. (v) The cell area for each individual cell in the population was obtained from a gamma distribution with standard deviation equal to 30% of the mean. (vi) When the age of a cell reaches the duration of its cell cycle, a division event occurs and a new cell with a peripheral remnant is generated. (vii) Based on the experimental data, we set the probability of conserving the remnant as a Hill function of the cell area, with a transition point at 200 μm². In the same way, the probability of transition from peripheral to central remnant (viii) and from central remnant to ciliary (ix) configurations were also set as Hill functions of the cell area at transition points of 400 and 200 μm², respectively. (x) The cell cycle length of each individual cell was obtained from a Hill function of the cell area with transition at 200 μm².

with PC biogenesis, indicating that the remnant is necessary for the latter to occur. Our model explains PC biogenesis in epithelial MDCK cells as a sequential process by which the daughter cell that inherits the midbody remnant forms a PC in a cell area–dependent manner. This process involves the movement of the remnant along the apical surface to enable the centrosome to form a primary cilium once the remnant and the centrosome become proximal. In addition to revealing the process of ciliogenesis in polarized epithelial cells, which was our primary objective, we made the unexpected but significant discovery that the postmitotic midbody is involved in this process.

Previous studies established that although the cleavage furrow in polarized epithelial cells initiates coincidently at the apical and basal surfaces, the rate of furrow ingression is more rapid from the basal surface. This difference in the rate of ingression causes the intercellular bridge to form close to the apical surface, near tight junctions (Reinsch and Karsenti, 1994; Morais-de-Sá and Sunkel, 2013). Consistent with these studies, we observed that cytokinesis does not occur at the middle region of the daughter cells but at the apical membrane of MDCK cells. Completion of cytokinesis requires both membrane and microtubule severing, the two processes being tightly correlated with abscission time (Steigemann et al., 2009; Chen et al., 2012). Severing the intercellular bridge can be symmetrical, when the abscission event takes place on both sides of the midbody, or asymmetrical, when it occurs only on one side. In the former case, the midbody is released, whereas the latter gives rise to asymmetrical midbody inheritance as one of the daughter cells receives the midbody remnant (Mierzwa and Gerlich, 2014; Dionne et al., 2015). A previous study showed that disassembly of the microtubule bundles of the intercellular bridge takes place on both sides of the midbody in epithelial MDCK cells (Elia et al., 2011). Although no large membrane bridge remnants were detected in that study by differential interference contrast microscopy, the technique cannot rule out the existence of a thin tether of plasma membrane connecting the midbody remnant to the rest of the cell. Our analysis of serial EM sections showed that this does occur in MDCK cells because peripheral and central remnants appear continuous with the tether, although the high contrast of the electrodense region with the density of the stalk might lead to the mistaken interpretation that they are discontinuous if only a few sections are examined. One possible explanation of this finding is that the severing of the membrane bridge on the side of the cell that inherits the remnant does not take place and that a thin tether with the rest of the cell is maintained during the movement of the remnant and in central remnants. A second scenario, which we consider less probable, is that severing of the plasma membrane is completed on both sides but that the midbody remnant remains on the cell surface and fuses thereafter with a thin protrusion of the cell.

The choice between release, conservation, or degradation of the midbody remnant depends on cell type and status (Marzesco

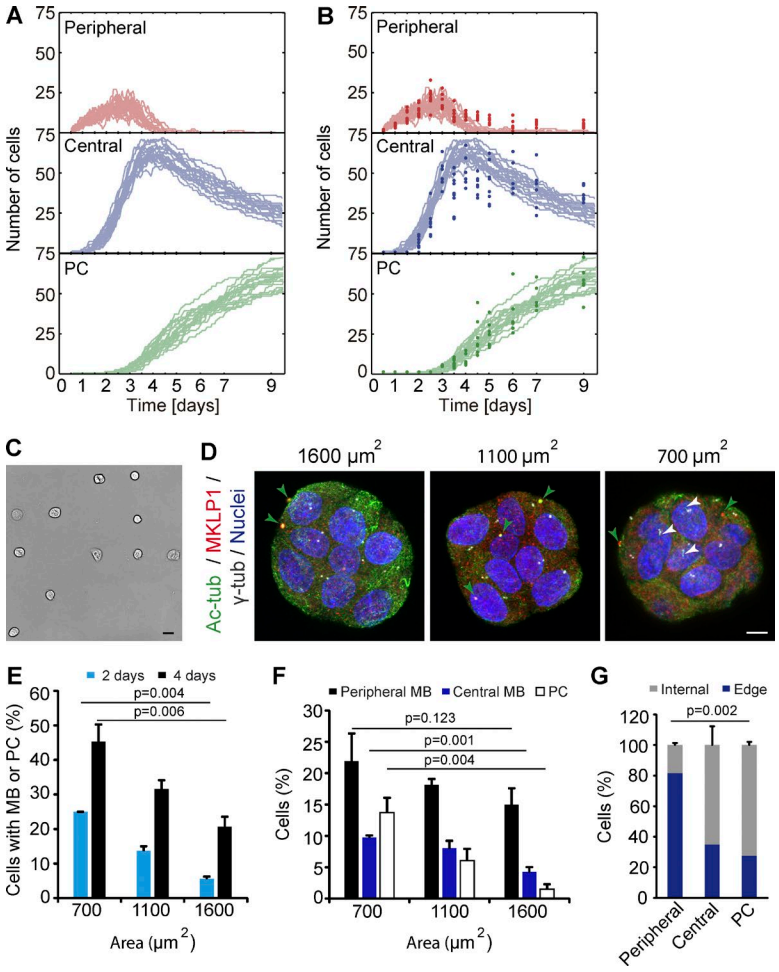

Figure 8. **Primary ciliogenesis in MDCK cells is governed by constraints in cell area at the single-cell level.** (A and B) Simulations (A) and superimposition of the experimental data (dots) shown in Fig. 1 F and the simulations (B). (C–E) A single cell per disk was seeded on disk micropatterns of 700, 1,100, and 1,600 μm² (C) and incubated for 2 or 4 d to allow the colony to reach a size of four or eight to 12 cells, respectively (D). (D) Cells were then processed for immunofluorescence analysis with antibodies to acetylated tubulin (Ac-tub), MKLP1, and γ-tubulin (γ-tub). Disk micropatterns with 8–12 cells are shown. The green and white arrowheads indicate the midbody remnant and PC, respectively. Nuclei were stained with DAPI. Bars: (C) 40 μm; (D) 6 μm. (E) The percentage of cells with either a midbody remnant or a PC relative to the total number of cells was determined after 2 or 4 d. Data represent the mean + SEM from three independent experiments (n = 180 cells grown for 2 d and n = 524 cells grown for 4 d were analyzed from 45 disk micropatterns each; Student's t test). (F) The percentage of cells with a peripheral remnant, a central remnant, or a PC relative to the total number of cells was determined after 4 d. (G) The cells at the edge or in internal positions on 700-μm² micropatterns were analyzed for the presence of peripheral or central midbody remnants or a PC after 4 d. The results are expressed as the percentage of internal or edge cells with peripheral or central remnants or a PC relative to the total number of cells with the corresponding structure. Data in F and G represent the mean + SEM from three independent experiments (n = 176 cells analyzed from 15 disk micropatterns; Student's t test).

et al., 2005; Pohl and Jentsch, 2009; Kuo et al., 2011; Salzmann et al., 2014), implying that its fate should be tightly regulated (Chen et al., 2013; Dionne et al., 2015). More than one remnant accumulates in subpopulations of stem cell–like populations and cancer cells, the frequency being higher in the latter (Ettinger et al., 2011; Kuo et al., 2011). Stem cells and cancer cells enriched in midbody remnants exhibit increased reprogramming efficiency and in vitro tumorigenicity, respectively (Kuo et al., 2011). We observed that partial remnant loss occurs in MDCK cells during the rapid regimen of cell division. In contrast, conservation takes place thereafter, coinciding with the switch to a slow regimen of cell proliferation. If the remnant is to be lost, the tether must be severed, whereas it can remain uncut in the case of conservation, as appears from our EM analysis of peripheral and central remnants. Therefore, according to our model, the cell area regulates the loss or conservation of the remnant and thereby the severing of the remnant stalk. Shedding of membranous particles with midbody markers has been observed in neural progenitors, although no relationship between those particles and PC biogenesis was established (Dubreuil et al., 2007). The endosomal sorting complex required for transport has a decisive role in the scission event of the intercellular bridge membrane that leads to daughter cell separation (Chen et al., 2012; Fededa and Gerlich, 2012; Agromayor and Martin-Serrano, 2013). The loss of the midbody remnants in the final stages of PC formation and during the rapid regimen of MDCK cell division implies scission of the thin stalk that connects the remnants to the rest of the cell. Therefore, it is plausible that the endosomal sorting complex required for transport machinery also mediates severing in both these occasions.

It was striking that, coinciding approximately with the establishment of cell–cell contacts, the midbody remnant moved along the apical membrane from the periphery to a central position in MDCK cells. Remnant movement in the plane of the plasma membrane has been observed after abscission in HeLa cells (Gromley et al., 2005). Because in MDCK cells a thin stalk appears to connect the peripheral and central remnants to the rest of the cell, it is feasible that the stalk mediates the movement of the remnant to encounter the centrosome. We observed that this movement was impaired in Rab8-knockdown cells. This observation does not necessarily means that Rab8 is directly involved in the process but rather that Rab8 expression is required for it to take place. Although we cannot rule out other possibilities such as a role of Rab8 controlling the cytoskeleton, since the best known function of Rab8 relates to membrane trafficking (Peränen, 2011; Barr, 2013), one possibility is that the effect of Rab8 knockdown on the movement of the remnant is likely caused by defects in the transport of proteins and/or lipids to the remnant zone that facilitate its movement.

We have observed accumulation of IFT subunits at the intercellular bridge, and previous studies have established the presence of exocyst subunits (Gromley et al., 2005) and Rab8 (Kaplan and Reiner, 2011). Because postmitotic midbodies contain these and other proteins known to be important in ciliogenesis and because the proteomes of midbodies (Skop et al., 2004) and PCs (Ishikawa et al., 2012) have a high degree of

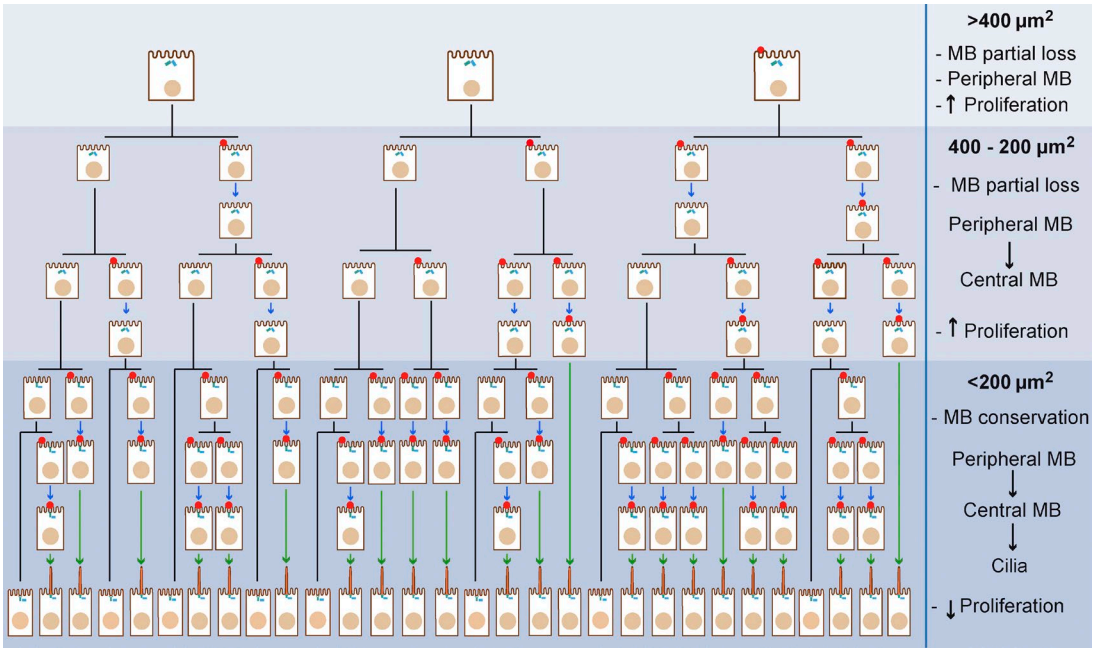

Figure 9. **Schematic of the proposed model of primary ciliogenesis in polarized epithelial cells.** The transitions of the midbody remnant (release or movement to a central position) and the beginning of the ciliogenesis process are controlled in a cell area–dependent manner by two cell area thresholds: a first threshold of ∼400 and a second of ∼200 µm². For cell areas above the second threshold, the remnant is only partially conserved, whereas it is fully conserved for cell areas below it. With regard to the remnant location, it locates peripherally in the apical surface at cell areas above a first threshold. When the area of the cell is between the first and a second threshold, it moves toward the center of the apical membrane to meet the centrosome, and this transition generates a pool of cells ready to start ciliogenesis. When the area of the cells falls below the second threshold, cells continue dividing and generating new midbody remnants that move to the cell center and enable ciliogenesis. Successive cycles of cell division (only one cycle is represented) increase the number of cells with a midbody remnant and, subsequently, the number of ciliated cells. In this way, the percentage of nonciliated cells becomes progressively smaller. Cell area reduction is produced by occupancy of the room of the mother cell by the daughter cells or compression of a cell by cells that divide in its proximity. Black lines represent cell divisions; blue and green arrows represent midbody remnant transitions (loss or peripheral to central movement) and PC formation, respectively.

overlap (Smith et al., 2011), one interesting possibility is that the connection of the remnant through the stalk facilitates the transfer of relevant material to the centrosome, once they are proximal. We have detected the establishment of a thin microtubular connection between the remnant and the centrosome when the two organelles meet at the center of the apical surface (Fig. 5 A). This connection can facilitate transport of material or can be itself the means by which the midbody remnant enables the centrosome for PC formation. A second possibility for the role of the remnant in ciliogenesis is that, because the PC has compact membranes at the ciliary base (Vieira et al., 2006) and these specialized membranes are required for PC formation (Reales et al., 2015), the stalk zone constitutes a compact membrane domain used to form the ciliary base. A third possibility is that the presence of the remnant proximal to the centrosome promotes the signaling required for primary ciliogenesis.

We focused on the cell area in our analysis because it is easily and directly measured. Cells sense their chemical and mechanical context and divide when they sense space is available (Puliafito et al., 2012). Such behavior appears to be achieved by coupling cell division to cell distortion and to changes in the balance of mechanical forces within the cell (Huang and Ingber, 1999). In subconfluent cell culture conditions, cells are not physically constrained by their neighbors, the cells are extended and subjected to tensile stress, and no PC is formed (Pitaval et al., 2010). However, under conditions of limited cell area brought about by cell proliferation, cells become progressively constrained by their neighbors and compressive stress replaces tensile stress (Trepat et al., 2009; Bazellières et al., 2015). In accordance with this, we observe that the movement of the midbody remnant from a peripheral position to a central position takes place as the cell grows in height and reduces its area (Fig. 3 C). We also demonstrate that cells grown on disk micropatterns show a greater percentage of PCs and central remnants in cells occupying an internal position relative to the cells at the disk edge. This observation shows the importance of cell–cell contacts in the transitions of the remnants and the formation of a PC. In contrast, primary ciliogenesis by the intracellular route takes place efficiently in RPE1 cells in the absence of cell–cell contact (Pitaval et al., 2010). The events leading to reduction in cell area, increase in cell height, and movement of the midbody remnant as well as cell polarization and junction formation are probably related with a common cause in a way that becomes evident only when tight cell–cell contacts are established. We propose that the change from tensile to compressive forces caused by cell–cell contacts in highly confluent MDCK cells (Ishikawa and Marshall, 2014), rather than the cell area per se, is the trigger at least for the conservation of the midbody remnant, its transition to a central position, and the beginning of ciliogenesis.

A relationship between the mother centriole and the intercellular bridge has been documented (Piel et al., 2001; Jonsdottir et al., 2010). In HeLa cells and L929 fibroblasts, the mother centriole moves transiently to the cell periphery to become proximal to the intercellular bridge before abscission and then moves back to the cell center (Piel et al., 2001). Centriole movement

was found to be highly dependent on cell line (Jonsdottir et al., 2010). Under certain conditions, the mother centriole was found even inside the intercellular bridge, very proximal to the midbody. The exocyst (Gromley et al., 2005), Rab8 (Kaplan and Reiner, 2011), and IFT subunits (Fig. S1, F–H) are present in the intercellular bridge. Therefore, it is plausible that, in addition to enabling cytokinesis completion as was originally proposed (Piel et al., 2001), the mother centriole recruits these or other materials from the midbody in some cell types. These materials could work in conjunction with membranes obtained from the Golgi or, as reported in neuroepithelial cells (Paridaen et al., 2013), with remnants of the ciliary membrane of the mother cell to form the ciliary vesicle in cells relying on the intracellular pathway of ciliogenesis. In cells in which the postmitotic midbody follows the autophagic route, materials from the remnant could also contribute to form the ciliary vesicle.

Our model of cilium formation is tightly linked to cell division, a process so inherent to life that the same basic mechanism of ciliogenesis that we propose could conceivably have operated early on in ciliary evolution using remnants of a primitive, microtubule-containing intercellular bridge. This view is somehow reminiscent of the model of Satir et al. (2007), which proposes that the evolutionary origin of the cilium is a microtubule-containing virus instead of the bridge remnant, as in our model.

The three microtubule-based organelles—the centrosome, the cilium, and the midbody—were discovered in the second half of the 19th century. The link between the centrosome and cell division was soon realized and subsequently thoroughly investigated, whereas research into the other two organelles has intensified only in recent years. Our finding that the postmitotic midbody enables PC formation reveals an unexpected role of the midbody in primary ciliogenesis and highlights a new biological mechanism that functionally links the midbody with the other two microtubule-based organelles.

Materials and methods

Antibodies and reagents

The sources of the antibodies to the different markers were as follows. IFT20 (rabbit polyclonal; used at 1/200; HPA021376), γ-tubulin (rabbit polyclonal; used at 1/2,000; T3559); mouse mAb IgG1 (clone GTU-88; used at 1/2,000; T6557), total α-tubulin (mouse mAb IgG1, clone DM1A; used at 1/500; T9026), and Rab8 (rabbit polyclonal; used at 1/500; R5530) used in immunoblotting experiments were obtained from Sigma-Aldrich. Rab8 (mouse mAb IgG2b, clone 4/Rab4; used at 1/100; 610844) used for immunofluorescence analysis was obtained from BD. Tyrosinated α-tubulin (rat mAb IgG2a, clone YL1/2; used at 1/500; MA1-80017) was purchased from Thermo Fisher Scientific. Exo70 (mouse mAb IgG2b, clone 70X13F3; used at 1/200) was purchased from Kerafast. Podocalyxin/gp135 (mouse mAb IgG1; used at 1/500; 3F2/D8) and ZO-1 (rat mAb IgG1; used at 1/500; R26.4C) were purchased from Developmental Studies Hybridoma Bank. MKLP1 (rabbit polyclonal; used at 1/500; sc-867) and β-catenin (rabbit polyclonal; used at 1/500; sc-7199) were obtained from Santa Cruz Biotechnology, Inc. PRC1 (mouse mAb IgG2b, clone 16F2; used at 1/200; MA1-846), IFT88 (rabbit polyclonal; used at 1/100; 13967-1-AP), and IFT81 (rabbit polyclonal; used at 1/100; 11744-1-AP) were obtained from Proteintech. Hepatocyte growth factor (product GF116) was obtained from EMD Millipore. DAPI stain was purchased from Thermo Fisher Scientific. Fluorescent phalloidin and secondary antibodies conjugated to Alexa Fluor 488, 594, or 647 were purchased from Invitrogen.

Cell culture

Epithelial canine MDCK II (CRL2936), IMCD3 (CRL2123), and RPE1 (CRL4000) cells were obtained from ATCC. Cells were grown in MEM supplemented with 5% FBS (Sigma-Aldrich) at 37°C in an atmosphere of 5% CO_2. Mycoplasma testing was regularly performed. For immunofluorescence analysis, 5.0×10^5 cells were seeded on 12-mm polycarbonate membranes of 0.2-µm pore size (Costar Transwell; Corning). For the quantitative analyses in Figs. 1 F, 7 (A–C), and S5 (C–E), 2.5×10^4 MDCK cells were plated onto coverslips maintained in 24-well multiwell plates and grown for the indicated times. Under these conditions, a mean of 18 cells per field were visualized with a 63× objective under our microscope 12 h after plating. Cells were then analyzed for α- and γ-tubulin staining and by differential interference contrast microscopy. Cells with both a PC and midbody remnant were assigned to the PC group. We cannot rule out that a small fraction of short PCs were scored as central midbody remnants in Fig. 1 F.

DNA constructs, siRNA, and transfection conditions

The DNA constructs expressing dsRed-centrin2 (Tanaka et al., 2004; plasmid 29523; Addgene) and GFP-PRC1 (Hu et al., 2012) were gifts from J. Gleeson (University of California, San Diego, La Jolla, CA) and C.-K. Hu (University of Stanford, Stanford, CA), respectively. The constructs expressing GFP- or cherry-tubulin were obtained from Takara Bio Inc. For transient transfection of DNA constructs, cells were transfected with Lipofectamine 2000 (Thermo Fisher Scientific) according to the manufacturer's recommendations. The construct expressing GFP-IFT20 was generated by cloning the IFT20 coding sequence, which was obtained by PCR using specific primers and human IFT20 cDNA (IMAGE clone 3907361; Source Bioscience) as template, in the pEGFP-C1 expression vector (Takara Bio Inc.). Stably transfected cells were generated by transfection and selection with 1 mg/ml G-418 (Thermo Fisher Scientific). The resulting clones were screened under a fluorescence microscope. 1.0×10^6 cells were transfected with 20 nM siRNA negative control (siC) Hi GC (product 12935-500) or 20 nM siRNA targeted to Rab8a (siRab8, 5′-GACAAGUUUCCA AGGAACG-3′) or IFT88 (siIFT88, 5′-UCGUCUAAGGCAAAU GGAACGUGAA-3′; Thermo Fisher Scientific) by electroporation in an Amaxa apparatus running the L-005 program. After overnight incubation, cells were washed three times and resuspended in fresh medium. Rab8 and IFT88 knockdown was verified by immunoblotting 72 h after transfection.

Immunofluorescence and time-lapse microscopic analyses

Cells were fixed in formalin for 20 min, rinsed, and treated with 10 mM glycine in PBS for 5 min to quench the aldehyde groups. Cells were then washed, permeabilized or not with 0.1% Triton X-100 in PBS at 4°C for 10 min, rinsed, incubated with 3% (wt/vol) BSA for 15 min, and incubated with the primary antibody. For γ-tubulin staining, cells were fixed with cold methanol for 5 min. After 1 h at room temperature, cells were washed and incubated with the appropriate fluorescent secondary antibody. For double-labeling experiments, the same procedure was repeated for the second primary antibody. Cells were mounted in coverslips using ProLong Gold antifade reagent (Thermo Fisher Scientific). For selective labeling of the apical surface, 0.25 mg/ml sulfo-NHS-biotin (Thermo Fisher Scientific) were added to confluent monolayers of MDCK cells. After 30 min at 4°C, the solution was removed and the remaining unreacted biotin was quenched by incubation with ice-cold serum-free MEM. The biotin groups were detected by incubation with streptavidin–Alexa Fluor 555 (Thermo Fisher Scientific) for 30 min. Images were obtained using an LSM 710 confocal microscope (ZEISS) with a 63× oil objective and a numerical aperture of 1.4. The projection of one to three apical planes is shown in the XY

images of cells grown on Transwells. For time-lapse fluorescence microscopy, we used a Nikon A1R confocal microscope with 60× water objective and a numerical aperture of 1.2. For 3D reconstruction, we used NIS-Elements microscope imaging software (Nikon). Cells were plated onto 35-mm glass-bottom dishes (MatTek) and maintained at 37°C in MEM without phenol red supplemented with 0.25% fetal bovine serum during the recording. Immunofluorescence and time-lapse experiments were performed at least four independent times, and images shown are representative from samples that were used for quantification. Brightness and contrast were optimized with ImageJ (National Institutes of Health) and Photoshop (Adobe Systems). Quantifications were performed using ImageJ.

Electron microscopy and 3D reconstruction

Cells grown on Transwell filters were fixed with 4% paraformaldehyde and 2% glutaraldehyde for 90 min at RT. Cell samples were then processed for embedding in Epoxy, TAAB 812 Resin (TAAB Laboratories) according to standard procedures. The samples were processed for sequential 80-nm ultrathin sections perpendicular to the plane of the cell monolayer. The obtained sections were numbered as S1 onwards. Sections were stained with saturated uranyl acetate and lead citrate by standard procedures. Samples were examined at 80 kV in an electron microscope (JEM-1010; Jeol). Pictures were taken with a TemCam-F416 (4,000 by 4,000-pixel) digital camera (TVIPS). For 3D reconstruction (Fig. 3 E and Video 5), EM images from a stack of 21 sequential sections (Fig. S3 B) were binned twice to give an effective pixel size at the specimen level of 4 nm. The EM image series were aligned with the IMOD software tool (Kremer et al., 1996). Structural features that were unequivocally identified in adjacent sections, with a particular focus on microvilli and discernible cytoplasmic structures, were manually selected and used as fiducial markers to guide the alignment. Full linear transformation was used to align each pair of successive sections independently. The 3D reconstruction was finalized by transforming each section into a common alignment in which the section located in the middle of the stack acted as a reference. The 3D reconstruction was modeled with IMOD by manually tracing the contour of the features of interest, particularly midbody remnants, plasma membrane, and microvilli along the sections of the EM stack (Fig. S3 B). The modeled reconstruction was visualized in 3D by surface rendering (Fig. 3 E and Video 5). As individual sections had a nominal thickness of 80 nm and we used a stack of 21 sections, the total thickness of the 3D reconstruction was ∼1.68 µm.

Midbody remnant removal

A mixed population of cells stably expressing or not expressing GFP-tubulin, which was used to visualize the midbody remnant, were grown for 4 d to generate a confluent monolayer. By using a glass pipette hitched to a patch-clamp equipment, remnants were removed by aspiration by TUSP (Video 7). Cell visualization was performed with a microscope (BX51; Olympus), using bright field and epifluorescence illumination. TUSP was assisted with Sutter MP-225 motorized micromanipulators. As a control, TUSP was applied to cells in a zone of the plasma membrane distant from the remnant. Cells were fixed 24 h post-TUSP and analyzed for the presence of PC. TUSP was performed on cells within areas previously labeled in the coverslips. The fluorescence pattern of the cells in the same area served to unambiguously identify TUSP-treated cells.

Micropatterned cell culture

MDCK cells were cultured on micropatterned glass coverslips (CYT OOchips; CYTOO). Disk-shaped micropatterns of different area (700, 1,100, and 1,600 µm^2) were used. 35,000 cells/chip were seeded and then washed and incubated according to the manufacturer's instructions.

Statistical analysis

In Fig. 6 C, χ^2 test was used because of the categorical nature of the data. Data in the rest of the figures were analyzed using Student's *t* test.

Mathematical model

Calculation of cell cycle duration and Hill coefficient for the mean proliferation dynamics of the population. The number of cells over time follows the equation

$$A(t) = A(0)2^{t/T(t)}, \quad (1)$$

where $A(t)$ is the number of cells at any given time t, $A(0)$ is the initial number of cells, and $T(t)$ is the mean cell cycle in the population that can change over time. Plot of the total number of cells over time (Fig. 7 B, black dots) from multiple experiments showed two distinct regimes of cell proliferation dynamics with a transition of 2.5–3.0 d. These "fast" and "slow" regimes can be fitted to Eq. 1 for constant values of the duration of the cell cycle of 0.85 and 22 d, respectively (Fig. 7 B, dashed gray lines). The long duration of the cell cycle calculated for this regimen can be explained in biological terms by assuming that all the cells divided slowly instead of a small proportion doing so at a normal rate. For the cell population model, cell cycle length $T(t)$ is assumed to follow a Hill function of the form

$$T(t) = \frac{T_{\max} + (T_{\min} - T_{\max})}{1 + \left(\frac{t}{S}\right)^h} \quad (2)$$

between minimum ($T_{\min}$ = 0.85 d) and maximum ($T_{\max}$ = 22 d) values, where S is the transition point. The transition point (2.68 d) was calculated as the intersection between the two dashed gray lines. The cell area at the transition point (212 µm^2) was estimated by dividing the total cell area (15,647 µm^2; see next paragraph) by the number of cells in the system predicted by Eq. 1 at 2.68 d. The Hill coefficient h (a measure of the sharpness of the transition between the fast- and slow-proliferating regimes shown in Fig. 7 B) was calculated by directly fitting Eq. 1 to the experimental value of the total number of cells for different values of h. The calculated number of cells (Fig. 7 B, solid black line) provided a good fit of the experimental data for values of $h > 100$, which corresponds to a very sharp transition in the mean cell cycle duration of the cell population. For simplicity, the same value (h = 100) of the Hill coefficient was used for the other Hill functions in the cell population–based simulation.

Calculation of the individual cell area in the simulations. The effective total area occupied by the cells was estimated from data from single-cell area measurements at days 6, 7, and 9 by multiplying the mean cell area at each time by the total number of cells present at those times. The mean of the three values was used to calculate the total area (15,647 µm^2) occupied by the cells (Fig. S5 D). The single-cell measurements of cell area for a population of cells at any time fitted to a gamma distribution with a 30% SD from the mean value at each time (as an example, see Fig. S5 E for day 2). Based on this observation, we set the area of each cell in the simulation as a random value sampled from a theoretical gamma distribution calculated for each time point by dividing the total area occupied by the number of cells at each time point (Fig. S5 C, small dots). The experimental mean cell area was calculated by dividing the effective area of the system by the mean number of cells at each time point (Fig. S5 C, large dots).

Calculation of the number of cells that conserve the midbody remnant. A newly formed midbody remnant with a peripheral distribution is inherited by one of the daughter cells after cell division. However, our time-lapse microscopic analysis showed that cells could lose the remnant (Video 9). We also observed that cell divisions of a mother

cell with one remnant generated two daughter cells with one remnant each (Video 10). To estimate the number of cells that have a remnant, we plot the number of cells with a remnant or a PC versus the total number of cells in the population. The plot revealed the existence of two linear regimens (Fig. 7 C). For low total cell numbers, the slope of the linear fitting was 0.32, suggesting that a fraction of newly generated cells did not conserve the remnant. For high cell numbers, the slope is practically 1.0, which means that all the new cells conserved the remnant. The point where the two linear fittings cross (73 cells) gives the transition point between the two regimens. The cell area corresponding to this transition (214 μm^2) was obtained by dividing the effective total area occupied by the cells (15,647 μm^2) by the number of cells (73 cells). The value of 214 μm^2 for this transition was used for the numerical simulation of the system.

Cell population-based simulations of the system. Simulations were performed using a Matlab (MathWorks) script developed in-house. Each simulation proceeded as follows: an initial number of 18 cells (this value was obtained from the mean of the initial number of cells in the microscope field in the experiments of Fig. 1 F) without a midbody remnant are plated on day 0 of the simulation (Fig. 7 D, i). For each cell in the population, we set a value of its individual area as explained in "Calculation of the individual cell area in the simulations" (Fig. 7 D, v). Each given cell in the simulation undergoes mitosis as soon as its age exceeds its cell cycle duration (Fig. 7 D, vi).

Based on the experimental data, we set the various transitions observed (cell cycle length, midbody remnant conservation, movement of the remnant from a peripheral to a central position, and the start of ciliogenesis) in the form of Hill functions of the cell area. In this way, we eliminated the dependence of the transitions on the time elapsed since cells were plated.

For the cell cycle length, Eq. 2 was rewritten as

$$T(A) = \frac{T_{max} + (T_{min} - T_{max})}{1 + \left(\frac{A}{S}\right)^h},$$

where the inflection of the curve was set as the cell area at 2.68 d (S = 212 μm^2) and the Hill coefficient calculated earlier (h = 100; Fig. 7 D, x).

The probability that cells have a midbody remnant was also set as a Hill function of the cell area in the form

$$P(A) = \frac{P_{max} + (P_{min} - P_{max})}{1 + \left(\frac{A}{S}\right)^h},$$

where $P(A)$ is the probability of conserving the remnant per time step, and P_{max} and P_{min} are the maximum and minimum probability, respectively. The transition point was set as the cell area when the system contains 73 cells (S = 214 μm^2). The probability of conserving the remnant before the transition point was set as 0.3, based on the value of the slope of the linear fitting (value per time step = $0.3^{1/T}$ = 0.943). As time goes by, the increasing number of cells results in a reduction in the cell area (Fig. S5 C). After the transition point (that is, when the mean cell area is less than 214 μm^2), cells conserved the remnant (P_{max} = 1). The Hill coefficient was also assumed as being h = 100 (Fig. 7 D, vii).

Based on our experimental data (Fig. 7 A), the transition from a peripheral to a central remnant can take place if the cell area is less than 400 μm^2. In addition, cells with a central remnant can become ciliated if their area is less than 200 μm^2. The probabilities of these two transitions were also defined as Hill functions of the cell area, from a zero value to a constant probability that is modulated to fit the final number of cells in each configuration (Fig. 7 D, viii and ix). Each simulation produces a slightly different outcome in the population of cells because we introduce variability in the value of the cell area to represent the experimental distribution of cell areas (Fig. 8 A, solid lines). For the sake of simplicity, for the simulation the calculated values for the transition for cell cycle (212 μm^2) and the probability of conserving the remnant (214 μm^2) were set as 200 μm^2 (same the value of the cell area where the first cells with a PC appear). In this way, we simplified the system by using just two transition points: 200 and 400 μm^2.

Online supplemental material

Fig. S1 shows the distribution of ciliary markers in MDCK cells during interphase and in cytokinesis. Fig. S2 shows a complete series of EM sections of a peripheral midbody remnant and a second example of peripheral remnant. Fig. S3 shows a complete series of EM sections of a remnant proximal to the centrosome at the middle of the apical membrane. Fig. S4 shows controls of cell polarization of Rab8-knockdown cells, a complete series of EM sections of a remnant in Rab8-knockdown cells, and the dynamics of the remnant in IMCD3 cells. Fig. S5 shows controls of membrane integrity of TUSP-treated cells and measures of cell area over time. Video 1 shows the formation of the intercellular bridge at the apical surface and the inheritance of the postmitotic midbody. Videos 2–4 show the movement of the midbody remnant to the center of the cell. Video 5 shows a 3D reconstruction of the midbody remnant at the center of the apical membrane. Video 6 shows the dynamics of the remnant during PC formation. Video 7 shows an example of the TUSP procedure. Video 8 shows that cells whose midbody remnant is removed by TUSP remain viable. Videos 9 and 10 show examples of a cell that loses the remnant and of cells that conserve it and divide to give rise to two daughter cells with a remnant each. Online supplemental material is available at http://www.jcb.org/cgi/content/full/jcb.201601020/DC1. Additional data are available in the JCB DataViewer at http://dx.doi.org/10.1083/jcb.201601020.dv.

Acknowledgments

The expert technical advice of the Optical and Confocal Microscopy and Electron Microscopy Units of the Centro de Biología Molecular Severo Ochoa is gratefully acknowledged. We thank Laura Fernández-Martín for her excellent technical help and Milagros Guerra for her invaluable assistance in the preparation of the EM sections. We also thank Minerva Bosch-Fortea for helpful comments. We express our gratitude to Dr. D.A. Hoffman (National Institute of Child Health and Human Development, Bethesda, MD) and Dr. J.A. Esteban (Centro de Biología Molecular Severo Ochoa, Madrid, Spain) for the use of their patch-clamp equipment.

This work was supported by the following grants from the Spanish Ministerio de Economía y Competitividad/Fondo Europeo de Desarrollo Regional: BFU2012-32532 and BFU2015-67266-R to M.A. Alonso, BFU2014-53299-P to D.G. Miguez, and TIN2012-37483-C03-02 to J.F. Fernández. Grants from the Comunidad de Madrid (S2010/BMD-2305) to I. Correas and from Instituto de Investigaciones Sanitarias Jiménez Díaz to J. Millán are also acknowledged. M. Bernabé-Rubio and D.G. Miguez are the holders of a fellowship and a Ramón y Cajal contract (RYC-2010-07450), respectively, from the Ministerio de Economía y Competitividad. G. Andrés was supported by the Amarouto Program from the Comunidad de Madrid.

The authors declare no competing financial interests.

Submitted: 7 January 2016
Accepted: 29 June 2016

References

Agromayor, M., and J. Martin-Serrano. 2013. Knowing when to cut and run: Mechanisms that control cytokinetic abscission. *Trends Cell Biol.* 23:433–441. http://dx.doi.org/10.1016/j.tcb.2013.04.006

Alieva, I.B., and I.A. Vorobjev. 2004. Vertebrate primary cilia: A sensory part of centrosomal complex in tissue cells, but a "sleeping beauty" in cultured cells? *Cell Biol. Int.* 28:139–150. http://dx.doi.org/10.1016/j.cellbi.2003.11.013

Ang, A.L., H. Fölsch, U.-M. Koivisto, M. Pypaert, and I. Mellman. 2003. The Rab8 GTPase selectively regulates AP-1B-dependent basolateral transport in polarized Madin-Darby canine kidney cells. *J. Cell Biol.* 163:339–350. http://dx.doi.org/10.1083/jcb.200307046

Barr, F.A. 2013. Review series: Rab GTPases and membrane identity: Causal or inconsequential? *J. Cell Biol.* 202:191–199. http://dx.doi.org/10.1083/jcb.201306010

Bazellières, E., V. Conte, A. Elosegui-Artola, X. Serra-Picamal, M. Bintanel-Morcillo, P. Roca-Cusachs, J.J. Muñoz, M. Sales-Pardo, R. Guimerà, and X. Trepat. 2015. Control of cell-cell forces and collective cell dynamics by the intercellular adhesome. *Nat. Cell Biol.* 17:409–420. http://dx.doi.org/10.1038/ncb3135

Benmerah, A. 2013. The ciliary pocket. *Curr. Opin. Cell Biol.* 25:78–84. http://dx.doi.org/10.1016/j.ceb.2012.10.011

Bornens, M. 2012. The centrosome in cells and organisms. *Science.* 335:422–426. http://dx.doi.org/10.1126/science.1209037

Chen, C.-T., H. Hehnly, and S.J. Doxsey. 2012. Orchestrating vesicle transport, ESCRTs and kinase surveillance during abscission. *Nat. Rev. Mol. Cell Biol.* 13:483–488. http://dx.doi.org/10.1038/nrm3395

Chen, C.-T., A.W. Ettinger, W.B. Huttner, and S.J. Doxsey. 2013. Resurrecting remnants: The lives of post-mitotic midbodies. *Trends Cell Biol.* 23:118–128. http://dx.doi.org/10.1016/j.tcb.2012.10.012

Das, A., and W. Guo. 2011. Rabs and the exocyst in ciliogenesis, tubulogenesis and beyond. *Trends Cell Biol.* 21:383–386. http://dx.doi.org/10.1016/j.tcb.2011.03.006

Dionne, L.K., X.-J. Wang, and R. Prekeris. 2015. Midbody: from cellular junk to regulator of cell polarity and cell fate. *Curr. Opin. Cell Biol.* 35:51–58. http://dx.doi.org/10.1016/j.ceb.2015.04.010

Dubreuil, V., A.-M. Marzesco, D. Corbeil, W.B. Huttner, and M. Wilsch-Bräuninger. 2007. Midbody and primary cilium of neural progenitors release extracellular membrane particles enriched in the stem cell marker prominin-1. *J. Cell Biol.* 176:483–495. http://dx.doi.org/10.1083/jcb.200608137

Elia, N., R. Sougrat, T.A. Spurlin, J.H. Hurley, and J. Lippincott-Schwartz. 2011. Dynamics of endosomal sorting complex required for transport (ESCRT) machinery during cytokinesis and its role in abscission. *Proc. Natl. Acad. Sci. USA.* 108:4846–4851. http://dx.doi.org/10.1073/pnas.1102714108

Ettinger, A.W., M. Wilsch-Bräuninger, A.-M. Marzesco, M. Bickle, A. Lohmann, Z. Maliga, J. Karbanová, D. Corbeil, A.A. Hyman, and W.B. Huttner. 2011. Proliferating versus differentiating stem and cancer cells exhibit distinct midbody-release behaviour. *Nat. Commun.* 2:503. http://dx.doi.org/10.1038/ncomms1511

Fededa, J.P., and D.W. Gerlich. 2012. Molecular control of animal cell cytokinesis. *Nat. Cell Biol.* 14:440–447. http://dx.doi.org/10.1038/ncb2482

Follit, J.A., R.A. Tuft, K.E. Fogarty, and G.J. Pazour. 2006. The intraflagellar transport protein IFT20 is associated with the Golgi complex and is required for cilia assembly. *Mol. Biol. Cell.* 17:3781–3792. http://dx.doi.org/10.1091/mbc.E06-02-0133

Gerdes, J.M., E.E. Davis, and N. Katsanis. 2009. The vertebrate primary cilium in development, homeostasis, and disease. *Cell.* 137:32–45. http://dx.doi.org/10.1016/j.cell.2009.03.023

Goetz, S.C., and K.V. Anderson. 2010. The primary cilium: A signalling centre during vertebrate development. *Nat. Rev. Genet.* 11:331–344. http://dx.doi.org/10.1038/nrg2774

Green, R.A., E. Paluch, and K. Oegema. 2012. Cytokinesis in animal cells. *Annu. Rev. Cell Dev. Biol.* 28:29–58. http://dx.doi.org/10.1146/annurev-cellbio-101011-155718

Gromley, A., C. Yeaman, J. Rosa, S. Redick, C.-T. Chen, S. Mirabelle, M. Guha, J. Sillibourne, and S.J. Doxsey. 2005. Centriolin anchoring of exocyst and SNARE complexes at the midbody is required for secretory-vesicle-mediated abscission. *Cell.* 123:75–87. http://dx.doi.org/10.1016/j.cell.2005.07.027

Heider, M.R., and M. Munson. 2012. Exorcising the exocyst complex. *Traffic.* 13:898–907. http://dx.doi.org/10.1111/j.1600-0854.2012.01353.x

Hildebrandt, F., T. Benzing, and N. Katsanis. 2011. Ciliopathies. *N. Engl. J. Med.* 364:1533–1543. http://dx.doi.org/10.1056/NEJMra1010172

Hu, C.-K., M. Coughlin, and T.J. Mitchison. 2012. Midbody assembly and its regulation during cytokinesis. *Mol. Biol. Cell.* 23:1024–1034. http://dx.doi.org/10.1091/mbc.E11-08-0721

Huang, S., and D.E. Ingber. 1999. The structural and mechanical complexity of cell-growth control. *Nat. Cell Biol.* 1:E131–E138. http://dx.doi.org/10.1038/13043

Ishikawa, H., and W.F. Marshall. 2014. Mechanobiology of ciliogenesis. *Bioscience.* 64:1084–1091. http://dx.doi.org/10.1093/biosci/biu173

Ishikawa, H., J. Thompson, J.R. Yates III, and W.F. Marshall. 2012. Proteomic analysis of mammalian primary cilia. *Curr. Biol.* 22:414–419. http://dx.doi.org/10.1016/j.cub.2012.01.031

Jiang, W., G. Jimenez, N.J. Wells, T.J. Hope, G.M. Wahl, T. Hunter, and R. Fukunaga. 1998. PRC1: A human mitotic spindle-associated CDK substrate protein required for cytokinesis. *Mol. Cell.* 2:877–885. http://dx.doi.org/10.1016/S1097-2765(00)80302-0

Jonsdottir, A.B., R.W. Dirks, J. Vrolijk, H.M. Ögmundsdottir, H.J. Tanke, J.E. Eyfjörd, and K. Szuhai. 2010. Centriole movements in mammalian epithelial cells during cytokinesis. *BMC Cell Biol.* 11:34. http://dx.doi.org/10.1186/1471-2121-11-34

Kaplan, A., and O. Reiner. 2011. Linking cytoplasmic dynein and transport of Rab8 vesicles to the midbody during cytokinesis by the doublecortin domain-containing 5 protein. *J. Cell Sci.* 124:3989–4000. http://dx.doi.org/10.1242/jcs.085407

Kremer, J.R., D.N. Mastronarde, and J.R. McIntosh. 1996. Computer visualization of three-dimensional image data using IMOD. *J. Struct. Biol.* 116:71–76. http://dx.doi.org/10.1006/jsbi.1996.0013

Kuhns, S., K.N. Schmidt, J. Reymann, D.F. Gilbert, A. Neuner, B. Hub, R. Carvalho, P. Wiedemann, H. Zentgraf, H. Erfle, et al. 2013. The microtubule affinity regulating kinase MARK4 promotes axoneme extension during early ciliogenesis. *J. Cell Biol.* 200:505–522. http://dx.doi.org/10.1083/jcb.201206013

Kuo, T.-C., C.-T. Chen, D. Baron, T.T. Onder, S. Loewer, S. Almeida, C.M. Weismann, P. Xu, J.-M. Houghton, F.-B. Gao, et al. 2011. Midbody accumulation through evasion of autophagy contributes to cellular reprogramming and tumorigenicity. *Nat. Cell Biol.* 13:1214–1223. http://dx.doi.org/10.1038/ncb2332

Latta, H., A.B. Maunsbach, and S.C. Madden. 1961. Cilia in different segments of the rat nephron. *J. Biophys. Biochem. Cytol.* 11:248–252. http://dx.doi.org/10.1083/jcb.11.1.248

Li, D., A. Mangan, L. Cicchini, B. Margolis, and R. Prekeris. 2014. FIP5 phosphorylation during mitosis regulates apical trafficking and lumenogenesis. *EMBO Rep.* 15:428–437. http://dx.doi.org/10.1002/embr.201338128

Marzesco, A.-M., P. Janich, M. Wilsch-Bräuninger, V. Dubreuil, K. Langenfeld, D. Corbeil, and W.B. Huttner. 2005. Release of extracellular membrane particles carrying the stem cell marker prominin-1 (CD133) from neural progenitors and other epithelial cells. *J. Cell Sci.* 118:2849–2858. http://dx.doi.org/10.1242/jcs.02439

Meder, D., A. Shevchenko, K. Simons, and J. Füllekrug. 2005. Gp135/podocalyxin and NHERF-2 participate in the formation of a preapical domain during polarization of MDCK cells. *J. Cell Biol.* 168:303–313. http://dx.doi.org/10.1083/jcb.200407072

Mierzwa, B., and D.W. Gerlich. 2014. Cytokinetic abscission: Molecular mechanisms and temporal control. *Dev. Cell.* 31:525–538. http://dx.doi.org/10.1016/j.devcel.2014.11.006

Mishima, M., S. Kaitna, and M. Glotzer. 2002. Central spindle assembly and cytokinesis require a kinesin-like protein/RhoGAP complex with microtubule bundling activity. *Dev. Cell.* 2:41–54. http://dx.doi.org/10.1016/S1534-5807(01)00110-1

Molla-Herman, A., R. Ghossoub, T. Blisnick, A. Meunier, C. Serres, F. Silbermann, C. Emmerson, K. Romeo, P. Bourdoncle, A. Schmitt, et al. 2010. The ciliary pocket: an endocytic membrane domain at the base of primary and motile cilia. *J. Cell Sci.* 123:1785–1795. http://dx.doi.org/10.1242/jcs.059519

Morais-de-Sá, E., and C. Sunkel. 2013. Adherens junctions determine the apical position of the midbody during follicular epithelial cell division. *EMBO Rep.* 14:696–703. http://dx.doi.org/10.1038/embor.2013.85

Nachury, M.V., A.V. Loktev, Q. Zhang, C.J. Westlake, J. Peränen, A. Merdes, D.C. Slusarski, R.H. Scheller, J.F. Bazan, V.C. Sheffield, and P.K. Jackson. 2007. A core complex of BBS proteins cooperates with the GTPase Rab8 to promote ciliary membrane biogenesis. *Cell.* 129:1201–1213. http://dx.doi.org/10.1016/j.cell.2007.03.053

Paridaen, J.T.M.L., M. Wilsch-Bräuninger, and W.B. Huttner. 2013. Asymmetric inheritance of centrosome-associated primary cilium membrane directs ciliogenesis after cell division. *Cell.* 155:333–344. http://dx.doi.org/10.1016/j.cell.2013.08.060

Peränen, J. 2011. Rab8 GTPase as a regulator of cell shape. *Cytoskeleton (Hoboken).* 68:527–539. http://dx.doi.org/10.1002/cm.20529

Piel, M., J. Nordberg, U. Euteneuer, and M. Bornens. 2001. Centrosome-dependent exit of cytokinesis in animal cells. *Science.* 291:1550–1553. http://dx.doi.org/10.1126/science.1057330

Pitaval, A., Q. Tseng, M. Bornens, and M. Théry. 2010. Cell shape and contractility regulate ciliogenesis in cell cycle–arrested cells. *J. Cell Biol.* 191:303–312. http://dx.doi.org/10.1083/jcb.201004003

Pohl, C., and S. Jentsch. 2009. Midbody ring disposal by autophagy is a post-abscission event of cytokinesis. *Nat. Cell Biol.* 11:65–70. http://dx.doi.org/10.1038/ncb1813

Pollarolo, G., J.G. Schulz, S. Munck, and C.G. Dotti. 2011. Cytokinesis remnants define first neuronal asymmetry in vivo. *Nat. Neurosci.* 14:1525–1533. http://dx.doi.org/10.1038/nn.2976

Puliafito, A., L. Hufnagel, P. Neveu, S. Streichan, A. Sigal, D.K. Fygenson, and B.I. Shraiman. 2012. Collective and single cell behavior in epithelial contact inhibition. *Proc. Natl. Acad. Sci. USA.* 109:739–744. http://dx.doi.org/10.1073/pnas.1007809109

Reales, E., M. Bernabé-Rubio, J. Casares-Arias, C. Rentero, J. Fernández-Barrera, L. Rangel, I. Correas, C. Enrich, G. Andrés, and M.A. Alonso. 2015. The MAL protein is crucial for proper membrane condensation at the ciliary base, which is required for primary cilium elongation. *J. Cell Sci.* 128:2261–2270. http://dx.doi.org/10.1242/jcs.164970

Reinsch, S., and E. Karsenti. 1994. Orientation of spindle axis and distribution of plasma membrane proteins during cell division in polarized MDCKII cells. *J. Cell Biol.* 126:1509–1526. http://dx.doi.org/10.1083/jcb.126.6.1509

Rodriguez-Boulan, E., G. Kreitzer, and A. Müsch. 2005. Organization of vesicular trafficking in epithelia. *Nat. Rev. Mol. Cell Biol.* 6:233–247. http://dx.doi.org/10.1038/nrm1593

Rohatgi, R., and W.J. Snell. 2010. The ciliary membrane. *Curr. Opin. Cell Biol.* 22:541–546. http://dx.doi.org/10.1016/j.ceb.2010.03.010

Rosenbaum, J.L., and G.B. Witman. 2002. Intraflagellar transport. *Nat. Rev. Mol. Cell Biol.* 3:813–825. http://dx.doi.org/10.1038/nrm952

Salzmann, V., C. Chen, C.Y.A. Chiang, A. Tiyaboonchai, M. Mayer, and Y.M. Yamashita. 2014. Centrosome-dependent asymmetric inheritance of the midbody ring in *Drosophila* germline stem cell division. *Mol. Biol. Cell.* 25:267–275. http://dx.doi.org/10.1091/mbc.E13-09-0541

Satir, P., C. Guerra, and A.J. Bell. 2007. Evolution and persistence of the cilium. *Cell Motil. Cytoskeleton.* 64:906–913. http://dx.doi.org/10.1002/cm.20238

Singh, D., and C. Pohl. 2014. Coupling of rotational cortical flow, asymmetric midbody positioning, and spindle rotation mediates dorsoventral axis formation in *C. elegans*. *Dev. Cell.* 28:253–267. http://dx.doi.org/10.1016/j.devcel.2014.01.002

Singla, V., and J.F. Reiter. 2006. The primary cilium as the cell's antenna: Signaling at a sensory organelle. *Science.* 313:629–633. http://dx.doi.org/10.1126/science.1124534

Skop, A.R., H. Liu, J. Yates III, B.J. Meyer, and R. Heald. 2004. Dissection of the mammalian midbody proteome reveals conserved cytokinesis mechanisms. *Science.* 305:61–66. http://dx.doi.org/10.1126/science.1097931

Smith, K.R., E.K. Kieserman, P.I. Wang, S.G. Basten, R.H. Giles, E.M. Marcotte, and J.B. Wallingford. 2011. A role for central spindle proteins in cilia structure and function. *Cytoskeleton (Hoboken).* 68:112–124. http://dx.doi.org/10.1002/cm.20498

Sorokin, S. 1962. Centrioles and the formation of rudimentary cilia by fibroblasts and smooth muscle cells. *J. Cell Biol.* 15:363–377. http://dx.doi.org/10.1083/jcb.15.2.363

Sorokin, S.P. 1968. Reconstructions of centriole formation and ciliogenesis in mammalian lungs. *J. Cell Sci.* 3:207–230.

Steigemann, P., C. Wurzenberger, M.H.A. Schmitz, M. Held, J. Guizetti, S. Maar, and D.W. Gerlich. 2009. Aurora B-mediated abscission checkpoint protects against tetraploidization. *Cell.* 136:473–484. http://dx.doi.org/10.1016/j.cell.2008.12.020

Tanaka, T., F.F. Serneo, C. Higgins, M.J. Gambello, A. Wynshaw-Boris, and J.G. Gleeson. 2004. Lis1 and doublecortin function with dynein to mediate coupling of the nucleus to the centrosome in neuronal migration. *J. Cell Biol.* 165:709–721. http://dx.doi.org/10.1083/jcb.200309025

Trepat, X., M.R. Wasserman, T.E. Angelini, E. Millet, D.A. Weitz, J.P. Butler, and J.J. Fredberg. 2009. Physical forces during collective cell migration. *Nat. Phys.* 5:426–430. http://dx.doi.org/10.1038/nphys1269

Vieira, O.V., K. Gaus, P. Verkade, J. Fullekrug, W.L.C. Vaz, and K. Simons. 2006. FAPP2, cilium formation, and compartmentalization of the apical membrane in polarized Madin-Darby canine kidney (MDCK) cells. *Proc. Natl. Acad. Sci. USA.* 103:18556–18561. http://dx.doi.org/10.1073/pnas.0608291103

Westlake, C.J., L.M. Baye, M.V. Nachury, K.J. Wright, K.E. Ervin, L. Phu, C. Chalouni, J.S. Beck, D.S. Kirkpatrick, D.C. Slusarski, et al. 2011. Primary cilia membrane assembly is initiated by Rab11 and transport protein particle II (TRAPPII) complex-dependent trafficking of Rabin8 to the centrosome. *Proc. Natl. Acad. Sci. USA.* 108:2759–2764. http://dx.doi.org/10.1073/pnas.1018823108

Wheatley, D.N., E.M. Feilen, Z. Yin, and S.P. Wheatley. 1994. Primary cilia in cultured mammalian cells: detection with an antibody against detyrosinated alpha-tubulin (ID5) and by electron microscopy. *J. Submicrosc. Cytol. Pathol.* 26:91–102.

Zuo, X., W. Guo, and J.H. Lipschutz. 2009. The exocyst protein Sec10 is necessary for primary ciliogenesis and cystogenesis in vitro. *Mol. Biol. Cell.* 20:2522–2529. http://dx.doi.org/10.1091/mbc.E08-07-0772